Article:

Paraskevopoulou, C orcid.org/0000-0002-7063-5592 and Diederichs, M (2018) Analysis of time-dependent deformation in tunnels using the Convergence-Confinement Method. Tunnelling and Underground Space Technology, 71. pp. 62-80. ISSN 0886-7798

https://doi.org/10.1016/j.tust.2017.07.001

Title: Analysis of Time-dependent Deformation in Tunnels using the Convergence-Confinement Method

Authors:

Chrysothemis Paraskevopoulou[1], Mark Diederichs[2]

Author Affiliations:

[1] School of Earth and Environment, University of Leeds, Leeds, UK

[2] Department of Geological Sciences and Geological Engineering, Queen's University, Kingston, Ontario, Canada

Key words:

long-term behaviour, time-dependency, creep, visco-elastic parameters

ABSTRACT

During the excavation of a tunnel the accumulated wall displacement and the loading of tunnel support is the result of both the tunnel advance (round length and cycle time) and the time-dependent behaviour of the surrounding rock mass. The current approach to analyze the tunnel wall displacement increase is based on the Convergence-Confinement Method (CCM) performed with either analytical (closed form solutions) or the usage of the Longitudinal Displacement Profiles. This approach neglects the influence of time-dependency resulting in delayed deformation that may manifest even minutes or hours after excavation. Failure to consider the added displacements in the preliminary design can result in false selecting the time of installation and the type of support system causing safety issues to the working personnel, leading to cost overruns and project delivery delays. This study focuses on investigating and analyzing the total displacements around a circular tunnel in a visco-elastic medium by performing an isotropic axisymmetric finite difference modelling, proposing a new yet simplified approach that practitioners can use taking into account the effect of time.

1 INTRODUCTION

Understanding the nature and origin of deformations due to an underground opening requires, as Panet (1993) noted, both knowledge of the rock-support interaction and interpretation of field data. Monitoring and measurement of tunnel wall displacements has shown that deformation initiates during excavation and may continue long after the tunnel construction is completed. This tunnel wall movement, also known as convergence, is the result of both the tunnel face advancement and the time-dependent behaviour of the rock mass. Many researchers (Fenner, 1938; Parcher, 1964; Lombardi, 1975; Brown et al. 1983; Corbetta et al. 1991; Duncan-Fama, 1993; Panet, 1993, 1995; Peila and Oreste, 1995; Carranza and Fairhurst, 2000, Alejano et al. 2009; Vrakas and Angnostou, 2014; Cai et al. 2015; Cui et al. 2015 etc.) have studied the interaction between the rock mass and the applied support. They have proposed various methodologies that are commonly used as a preliminary tool for quickly assessing the system behaviour (between the surrounding rock mass and support) during both the design and construction process of underground projects (Gschwandtner and Galler, 2009). In addition, most of these solutions are based on the well-known and widely used Convergence-Confinement Method (CCM). CCM is a two-dimensional simplified approach that can be used to simulate three-dimensional problems as the rock-support interaction in tunnels. More specifically, CCM is widely utilized to estimate the required load capacity of the proposed support system. The traditional approach of this methodology involves the Ground Reaction Curve and the Longitudinal Displacement Profile that when used in combination with the Support Characteristic Curve (SCC) they provide information on the required support load in regards to the tunnel face location as a percentage of the anticipated maximum tunnel wall displacement. Gschwandtner and Galler (2010) suggested a new approach for using the CCM while considering the time-dependent material of the support by investigating different support scenarios of rockbolts and shotcrete, investigating how the behaviour of the support system changes over time. However, even the more commonly applied simplified formulations of CCM do not explicitly capture the time-dependent component of rock mass deformation. Time-dependent closure, for instance due to creep, can have a significant impact on support loading. Failure to account for these additional loads and deformations can result in unexpected failures, causing safety issues for the working personnel, leading to cost overruns and project delivery delays.Questions of the applicability of such methods when dealing with time-dependent rheological rockmasses are addressed in this paper by investigating the total observed displacement on tunnel walls in an isotropic visco-elastic medium, taking into consideration both the tunnel advancement and cumulated deformation due to the rheological behaviour of the material over time.

1.1 Ground Reaction Curve (GRC) and Longitudinal Displacement Profile (LDP) Calculations

An important component of the CCM method is the Ground Reaction Curve (GRC). This is a characteristic line that records the decrease of an apparent (fictitious) internal (radial) support pressure, from the in situ pressure to zero when considering the unsupported case of a circular tunnel after excavation. This pressure reflects the tunnel excavation process as the tunnel is being excavated (out-of-section) past the section of interest and continues to be excavated beyond the reference position (usually the location of the tunnel face) as shown on the right part of Figure 1. The internal pressure (p_i) acts radially on the tunnel profile (from the inside) and represents the support resistance needed to hinder any further displacement at that specific location (Vlachopoulos and Diederichs, 2009). In reality, this pressure represents an idealized sum of the contribution of the nearby unexcavated tunnel core (surrounding rock mass) and any applied support installed and is zero for a fully excavated unsupported tunnel. The GRC depends on the rock mass behaviour. It is assumed to be linear for an elastic material but it varies if the material is elasto-plastic or visco-elastic etc. Many researchers have studied the GRC responses of different materials. For example, Brown et al. 1983, Alejano et al. 2009, Wang et al. 2010, Gonzales-Cao et al. 2013 have proposed analytical solutions for strain-softening rock masses based on different GRCs. Vrakas (2017) proposed a finite strain semi-analytical solution for the ground response problem of a circular tunnel in elasto-plastic medium with non-linear strength envelopes. Panet (1993) gives examples of GRCs of the most used visco-elastic models that are discussed in Section 2.2.

For elastic or moderately yielding rock masses approximately one third of the total displacement is observed at the tunnel face (Hoek et al. 2008) shown as x=0 on the right hand axis of Figure 1. The deformation initiates in front of the face (x<0), usually one to two tunnel diameters ahead of the face, and reaches its maximum magnitude at three to four tunnel diameters away from the face inside the tunnel (x>0).

A Longitudinal Displacement Profile (LDP) of the tunnel closure is a graphical representation of the progression of the tunnel wall displacement (radial) at the reference section as the tunnel advances to and beyond this section. The reference datum (x=0) indicates that the tunnel face is stationed at the reference section (Figure 1). LDPs are calibrated for a simplified unsupported tunnel and are then used in combination with the GRC to determine the support system required for the stability of the tunnel walls as well as the time of support installation.

Figure 1. The Ground Reaction Curve response of an elasto-plastic material and its relation to the LDP. Y-axis on the left refers to the internal pressure (p_i) normalized to the in-situ pressure (p_0), Y-axis on the right refers to the distance from the face (x) normalized to the tunnel radius (R) and X-axis refers to the radial displacement at a location x normalized to the maximum radial displacement.

It should be noted that in Figure 1 no time-dependent component is taken into consideration in this example.

LDPs are initially calculated using analytical solutions or numerical analysis. In two-dimensional numerical analysis, LDPs are calculated through two-dimensional axisymmetric models for homogeneous and isotropic initial stress condition circular tunnels. Table 1 summarizes the various analytical solutions proposed by researchers (Panet and Guenot, 1982; Corbertta et al. 1991; Panet, 1993, 1995; Chern et al. 1998; Unlu and Gercek, 2003; Vlachopoulos and Diederichs, 2009) to be used for LDP calculations according to the rock mass behaviour (i.e. elastic or elasto-plastic) where u_{max} refers to the maximum radial displacement attained R and x denote the tunnel radius and x the under-investigation location, v is the Poisson's ratio.

Table 1. Analytical solutions for LDP calculation depending on the medium.

Panet (1993, 1995) and Corbetta et al. (1991) derived relationships for the LDP profiles of elastic material behaviours. Panet and Guento (1982) Chern et al (1998) proposed relationships for elato-plastic materials. Unlu and Gercek (2003) are the first who noted that the LDP curve in front of the face (in the non-excavated rock mass where x<0) is different than the LDP curve in behind the tunnel face (in the already-excavated rock mass where x>0). At the tunnel face (where x=0) the radial displacement can be estimated using the Poisson's Ratio, as shown in Table 1. The same statement was used by Vlachopoulos and Diederichs (2009) who proposed three different equations to estimate the LDP for an elasto-plastic material in relation to the location x in terms of the tunnel face which is used for weak ground conditions at great depth assuming that a large ultimate plastic radius is created around the tunnel. It is important to note that none of the afore-ascribed LDP equations on Table 1 takes into consideration any deformation anticipated due to time-dependent squeezing (for instance). Additionally, any application of these LDPs equations to time-dependent rock masses will yield erroneous results leading to underestimation of the anticipated tunnel wall displacements and the support system requirements.

2 TIME-DEPENDENT BEHAVIOUR

The tendency of various rocks and rock masses to exhibit time-dependent shear deformation when subjected to a constant stress state (that it is less than the strength of the rock material) is known as creep. In tunnelling, creep behaviour emerges as the on-going increase of the radial displacements observed in the tunnel walls. This increase is related to the rheological properties and creep potential of the surrounding rock mass and can be considered to be in addition to the displacement resulting due to the incremental steps of tunnel advance - although the progress of the tunnel takes time and so this closure component is often but erroneously referred to as time-dependent (Paraskevopoulou, 2016). For the design of tunnels in rock masses at depth it is often important to account for creep. This consideration extends through the initial construction period and beyond. The time effect can contribute up to 70% of the total deformation (Sulem et al. 1987).

In tunnelling, time-dependent behaviour is often observed in weak rocks and rock masses that exhibit severe squeezing (Barla 2001, Barla et al. 2010). Squeezing in this case, results from the plastic displacements due to shearing over a long period of time which leads to apparent visco-plastic creep. However, brittle rocks can experience creep when subjected to high in situ stresses (Malan, 1997; Damjanac and Fairhurst, 2010) and can also be subject to long-term strength degradation due to crack growth over time with or without observable creep. Creep behaviour (Goodman, 1980) is usually characterized by three stages (primary, secondary, tertiary) that follow the instantaneous response due to the change in the boundary conditions (constant stress) shown in Figure 2. As the stress or load is kept constant, the accumulated strains increase with a decreasing rate (primary stage). When this primary stage subsides and the strain increase approaches a constant strain-rate, the transition to the secondary (or steady state) can then be evident (although the processes of secondary creep may act coincidentally during the primary stage). At the end of the secondary state, the strain rate accelerates yielding or even failing the material in a brittle manner, a delayed yield process referred to as tertiary creep (although the use of the term creep may not be accurate in all cases). This failure is the result of weakening of the rock mass during creep deformation or excess deformations that create unstable conditions. It should be also noted that the magnitude and duration of each stage depends on the type of the rock material. Ductile materials such as rock salt may never reach tertiary creep (yield) as they are more prone to deforming without yielding (creep processes do not create damage) whereas in brittle materials like granite the secondary stage of creep is not always observed as Lockner (1993) also reported. In these materials, the tertiary stage manifests as delayed yield under sustained loading between a lower bound crack initiation threshold and maximum strength.

Figure 2. Characteristic curve of creep behaviour.

2.1 Time-dependent Formulation and Rheological Models

Many researchers have developed and proposed various formulations and constitutive laws to capture the time-dependent behaviour of rock materials. Most formulations of time-dependent behaviour, suggested in the literature, can be separated into three main categories: a) empirical functions based upon curve fitting of experimental data (Mirza, 1978; Aydan et al. 1996; Sign et al. 1997; etc.), b) rheological functions based upon time-dependent behaviour models (Lo and Yuen, 1981; Aristorenas, 1992; Malan, 1997; Chin and Rogers, 1998; etc.), and, c) general theories (Perzyna, 1996; Debernardi, 2008; Sterpi and Gioda, 2009; Kalos, 2014; etc.) that are considered to be the most advanced aspects of numerical analysis codes (i.e. Finite Element and Finite Difference codes). The most commonly used of the three are the rheological models. They are based on constitutive relationships between stress and strain. In order to simulate the time-dependent viscous behaviour, usually elastic springs, viscous dashpots and plastic sliders are coupled in series or parallel. It is then possible to reproduce elasto-plastic, visco-elastic, visco-plastic, elasto-visco-plastic etc. mechanical behaviours. For simplicity here, it should be noted that at this paper focuses on the visco-elastic behaviour and no plastic yield is considered.

Table 2 summarizes the most common visco-elastic models used to simulate creep behaviour, where: σ=stress, ε=strain, E=Young's modulus, K=bulk modulus, G =shear modulus, η=viscosity, t=time, subscript K denotes Kelvin model, subscript M denotes Maxwell model, p is the mean stress and q is the deviatoric stress. Kelvin and most commonly its extension to the generalized Kelvin (Kelvin-Voigt) model comprised of a spring coupled in parallel with a dashpot is used to simulate the instantaneous response and primary stage of creep. Maxwell model or its extension (generalized Maxwell), a spring in series with a dashpot is used to capture the secondary creep stage. Coupling of these two models in series gives the Burgers model that is used to simulate the first two stages of creep behaviour. These models in order to be utilized, require the knowledge of creep parameters (i.e. viscosities (η) and shear moduli (G) of the mechanical analogues) that can be derived from creep tests in the laboratory (Lama and Vutukuri, 1978; Goodman, 1980) or in situ conditions (Goodman, 1980; Chen and Chung, 1996). According to Goodman, the visco-elastic parameters (η_K, η_M, G_K, G_M) can be estimated by fitting the experimental results of static load (creep) tests to the mathematical curve of the strain response of the Burgers model at different time increments and the corresponding strain intercepts.

Burgers-creep viscous (CVISC) model (Table 2) is a visco-elastic-plastic model introduced by Itasca (2011) and consists of the Burgers visco-elastic model in series with a plastic slider (Table 2). The plastic component is based on the Mohr-Coulomb failure criterion and it is used to pseudo-simulate the tertiary stage of creep. However, since the plastic slider is not coupled with a viscous dashpot plastic-yielding is independent of time and depends only on the stress (Paraskevopoulou and Diederichs, 2013). If the model is subjected to a stress above the yielding stress of the slider the model behaves as an elasto-plastic material whereas if it is stressed below the yielding threshold the model behaves similar to a Burgers body.

Commonly, Burgers model is preferable for practical applications (Goodman, 1980). It should be stated, however, that there is not a simple model that can describe all the creep stages satisfactorily and can be used for all rock types and all in situ conditions without limitations. For instance, heavily sheared rock masses can exhibit primary creep in normal stress conditions whereas high strength materials will not (Paraskevopoulou and Diederichs, 2013).

Table 2. Visco-elastic rheological models, their associated mechanical analogues, stress-strain and time-relationships.

(It should be noted that for incompressible materials E=3G).

2.2 Time-dependent Deformation in Tunnelling

The time-dependent response around the tunnel in a visco-elastic material has also been discussed in the literature. Analytical and closed form solutions that take into account the time-dependent convergence have been proposed in viscous medium for supported (i.e. Sakurai, 1978; Pan and Dong, 1991) and unsupported (i.e Panet, 1979; Sulem et al., 1987; Fahimifar, et al. 2010;) circular tunnels. Gnirk and Jonson (1964) analyzed the deformational behaviour of a circular mine shaft in a visco-elastic medium under hydrostatic stress. Goodman (1980) described a methodology on estimating visco-elastic creep parameters based on curve-fitting of tunnel data that experienced creep defromation. Yiouta-Mitra et al. (2010) investigated the LDP of a circular tunnel in a visco-elastic medium, neglecting however the effect on the cumulative tunnel wall displacement due to the tunnel advancement. Nomikos et al. (2011) performed axisymmetric analyses on supported tunnel within linear visoc-elastic rock masses. Although some of these formulations do consider the tunnel advance in the estimated total deformation, yet are found to be impractical due to the complex calculations required.

In this paper, the linear visco-elastic analytical solutions developed by Panet (1979) and proposed for the Kelvin-Voigt and Maxwell models, are utilized for the calculation of the time-dependent radial displacements of an unsupported circular tunnel. Fahimifar et al. (2010) developed a closed-form solution considering the time-effect when tunnelling within a Burgers material, this formulation is also adopted in the presented analysis. Table 3 summarizes the mathematical representations and expected material response due to time and more specifically creep behaviour; the visco-elastic models are presented as well as their analytical solutions and the radial displacement – time relationships, where: σ_o is the in situ stress, σ_r is the radial stress, u_r refers to the radial tunnel wall displacement, r is the tunnel radius, t describes the time, T denotes the retardation – relaxation time of each model, G is the shear modulus, η is the viscosity, t=time, subscripts K, M and ∞ refer to Kelvin-Voigt model, Maxwell model and the harmonic average, respectively.

Table 3. Visco-elastic models and analytical solutions for a circular unsupported tunnel. The analytical solutions for Kelvin-Voigt and Maxwell model are adopted from Panet (1979) and for Burgers from Fahimifar et al. (2010).

It should be noted that when time is assumed to be infinite the shear modulus used in the Kelvin model is estimated with the harmonic average G_∞ and is not equal with the initial shear modulus of the rock mass G_0.

2.3 Combining the two effects in a Longitudinal Displacement Profile (LDP)

The effects of tunnel advancement and time in the total radial displacements observed in the tunnel walls are shown in Figures 5 and 6 and expressed in the form of the LDP of an unsupported circular tunnel in an elasto visco-elastic-plastic and an elasto-visco-elastic medium respectively. In Figures 3 and 4, r is the tunnel radius, D is the tunnel diameter, t denotes the time, x denotes the distance from the tunnel face which is a function of time, u_r refers to the radial tunnel wall displacement which is the function of time and distance from the tunnel face, G is the shear modulus, η is the viscosity, q is the deviatoric stress, σ is the applied stress, subscripts M, K, y refer to Kelvin and Maxwell models and yielding threshold respectively; superscripts el, p, s and tet denotes the elastic response and primary, secondary and tertiary components of the creep behaviour, respectively. The former case (Figure 3) represents the case (elasto-visco-elastic-plastic) where the material undergoes all three stages of creep until ultimate failure. This response is expected in severe squeezing rock masses where the induced-creep behaviour leads the material to fracture and failure after exhibiting large deformations and noticeable convergence.

Figure 3. Longitudinal Displacement Profile (LDP) in an elasto-visco-elastic-plastic medium (see text for details).

Figure 4 illustrates the anticipated LDP of the tunnel displacement in an elasto-visco-elastic medium where no tertiary creep takes place. More ductile materials as in the case of rock salt can behave in such manner.

Figure 4. Schematic representation of the Longitudinal Displacement Profile (LDP) in an elasto-visco-elastic medium (see text for details).

In both Figures 3 and 4, it is shown that when no time-effect is considered, the total displacements are underestimated which can lead to erroneous calculations at the initial stages of the design process. Detailed investigation is recommended when dealing with rocks and rock masses that show time-dependent potential. The following discussion serves as an attempt to highlight the importance of time-dependent behaviour during tunnelling through a series of axisymmetric numerical analyses.

3 NUMERICAL ANALYSIS

An axisymmetric parametric analysis was performed within FLAC software (Itasca, 2011). The geometry of the model and the excavation sequence characteristics are shown in Figure 5. A circular tunnel of 6 m diameter and 400 m length was excavated in isotropic conditions. Full-face excavation was adopted. Two cases were assumed depending on the excavation step in each excavation cycle. In the first case (Case 1: D&B), the excavation step per cycle was 3 m as such conditions are considered to be typically representative of drill and blast excavation method on a fairly good quality rock mass. In the second case (Case 2: TBM), the excavation step per cycle was simulated to 1 m to represent the excavation sequence of a 6 m diameter mechanized tunnel using a TBM. The rock mass for both cases was assumed to behave as an elasto-visco-elastic material and CVISC model within FLAC software (Itasca, 2011) was employed. As previously discussed, the CVISC model is a visco-elastic-plastic model although for this purpose, the cohesion and tension on the model were given very high values to prevent any yielding from taking place in the model. No support measures were assumed on the study presented-herein.

Figure 5. Case 1 refers to drill and blast method with 3 m excavation step per cycle (Drill jumbo graphic courtesy of Fletcher & Co.), Case 2 refers to TBM (Tunnelling Boring Machine) method with 1 m excavation per cycle (TBM graphic courtesy of Herrenknecht AG).

In order to investigate further the time-dependent component of the total radial displacements it was decided to perform two main different analyses for both cases (D&B and TBM). The first analysis aimed to examine the contribution of primary creep using the Kelvin-Voigt model. In this regard, the viscous dashpots of the Maxwell body within the CVISC model was deactivated. On the second analysis, the contribution of the Burgers model was investigated in order to capture both primary and secondary stages of creep. In this case, both the Kelvin and the Maxwell bodies were activated.

In addition, three different sets of parameters were used for the three analyses on both cases shown in Table 4. However, for the scope of this study only the visco-elastic parameters varied between the three sets.

Table 4. Parameters used for CVISC model.

It should be stated that the visco-elastic parameters were chosen according to the analytical solution (Eq. 1) of the Kelvin-Voigt model developed by Panet (1979).

$$u_r = \frac{\sigma_o r}{2G_o} + \frac{\sigma_o r}{2G_K}\left[1 - \exp\left(-\frac{t}{T_K}\right)\right] \quad \text{(Eq. 1)}$$

where: σ_0 is the in-situ stress conditions, r is the tunnel radius, G_0 the elastic shear modulus, G_K is the Kelvin shear Modulus, η_K is Kelvin's viscosity and T_K is known as retardation time and it is the ratio of Kelvin's viscosity over the Kelvin shear Modulus.

It was observed that the relaxation (retardation) time of the Kelvin-Voigt model plays a key rolel as this parameter controls the curvature of Kelvin's behaviour. In other words, the retardation time of Kelvin shows how fast the model will converge and reach a constant value. In this regard, the visco-elastic parameters were chosen so the retardation time (T_K), found in the literature (Barla et al. 2010; Zhang et al. 2012; Feng et al. 2006) varies one order of magnitude between the three sets.

Furthermore, in order to take into consideration both the time-dependent component and the tunnel advance and examine their contribution to the total displacement recorded, the time of the excavation cycle was also captured in each set of parameters for both cases in the two analyses. The time of each excavation model varied from 2 to 8 hours. Additionally, two supplementary analyses were performed, one involved a set of runs with the Kelvin-Voigt model and the other a set of runs with the elastic models. These two analyses were used to validate the numerical models and were compared with analytical solutions. In total 62 models were simulated and their LDPs were analyzed and compared. Table 5 summarizes all the model runs performed in the presented parametric study.

Table 5. Nomenclature and model runs in this study.

4 NUMERICAL RESULTS

4.1 Comparison of Numerical Analysis with Analytical Solutions

The first step in this analysis was to compare the numerical results to the analytical solutions of the elastic (instantaneous deformation at each excavation step) and the Kelvin-Voigt model (hypothetically infinite time delay between each excavation step to allow full convergence of primary creep stage). Figure 6 shows that the numerical results are in agreement with the analytical solutions. It should be added that the elastic numerical case was compared to the elastic solution of Vlachopoulos and Diederichs (2009) assuming that no plastic radius occurs at the tunnel walls (i.e. r_p/r_t=1) The results from Kelvin-Voigt case were compared to Eq. 1.

Figure 6. (Left) Numerical results (solid lines) related to the analytical solutions (as referenced) for the elastic and the Kelvin Voigt model, (Right) closer representation of the data for x values of -15 < x < 25.

These results serve to validate the numerical model. The real question, however, is how the viscous behaviour impacts the LDP between the two extremes in Figure 6 as the elastic case represents instantaneous excavation (cycle time is effectively zero) while the fully converged Kelvin-Voight model (zero viscosity) represents an infinite cycle time between excavation steps. It is important, then, to consider the impact of the excavation rate (cycle time).

In order to examine the time-dependent potential during the construction, the tunnel excavation stages should be also considered. The bounding case numerical results (i.e. elastic and Kelvin-Voigt reference models) in the following sections were used as reference guides as they were considered to be the two extremes, the elastic is representative for the short-term LDP where no time-effect is considered whereas the Kelvin-Voigt is considered the long-term LDP during the primary stage of creep. From then on all of the results in the graphs refer to the numerical analyses unless otherwise stated.

The results are presented in two different ways shown in Figures 7 to 10. First, since the total displacement is much higher when the time component manifests, it was decided to normalize the total displacement to the maximum displacement of the Kelvin-Voigt reference model ($u_r\infty_{max}$), shown in the Figures on the left vertical axes. Second, the numerically computed displacement against the tunnel face location is also plotted (right vertical axes). It should be noted that in the following Figures x is the distance from the tunnel face, R is the tunnel radius, u_r is the absolute radial tunnel wall displacement, u_re_{max} is the maximum elastic displacement and $u_r\infty_{max}$ is the maximum visco-elastic displacement of the Kelvin-Voigt model. Grey and black lines are the elastic and the zero-viscosity KV models respectively.

4.2 KELVIN-VOIGT (KV), Investigating Primary Stage of Creep

The first main analysis involved the investigation due to the time-effect on the overall total tunnel wall displacement assuming that only primary creep is observed in addition to the effect of tunnel advancement. For this purpose, the Kelvin-Voigt model (with non-zero viscosity) was assumed to represent the primary stage of creep and was used to simulate the mechanical behaviour of an elasto-visco-elastic rock mass. The results for the drill and blast case and the TBM are presented in Figures 7 and 8, respectively.

Figure 7. (Left) Numerical results of LDPs for the drill and blast (DB) case of the KELVIN-VOIGT (KV) analysis (the hours on the legend denote hours per excavation cycle), (Right) closer representation of the data for x values of $-6 < X < 12$.

Figure 8. (Left) Numerical results of LDPs for the TBM case of the KELVIN-VOIGT (KV) analysis (the hours on the legend denote hours per excavation cycle), (Right) closer representation of the data for x values of $-2 < X < 4$.

Figures 7 and 8 show similar trends for the three sets of parameters. The results imply that increased cycle time or excavation delay exacerbates the mechanical behaviour of the rock mass, as in all models an increase of the ultimate total displacement was observed. This increase depends on the visco-elastic parameters of the Kelvin-Voigt model. Furthermore, it is shown that the models employed using the parameters of SET #2 and #3 which have a lower retardation time (T_K) reached a constant value sooner than the models of SET#1. As expected, an increase of the retardation time parameter will result in an increase of the time required by the model to reach a constant value and become time-independent.

The excavation method used and thus the step advancement (m/excavation cycle) influences the results. It was observed that the models simulated employing the TBM sequence (1 m advance) reached a constant displacement value closer to the excavation face than the ones observed in the Drill and Blast Case (3 m advance). This was expected as in these analyses the time in each excavation cycle is considered; consequently, the 1-m excavation per cycle completes less tunnel meters during the same period than the 3-m excavation step.

Finally, the duration of each excavation cycle is important. It is shown that the displacement during the 8-hour shifts reached a constant value closer to the tunnel face than the 2-hours shift. This is also reasonable as the elapsed-time during excavation cycles contributes in allowing the rock mass to deform and reach its maximum displacement value.

4.3 BURGERS (B), Investigating Primary and Secondary Stage of Creep

The second stage of this analysis was to investigate the influence of both primary and secondary stages of creep behaviour using the Burgers model. The results are presented in Figures 9 and 10 for the drill and blast and TBM case, respectively. Similar observations with the previous case of KELVIN-VOIGT analysis can be made.

The Burgers model simulates the idealized behaviour of the first two stages of creep. The maximum strains (deformation) due to the secondary stage (Maxwell model) are effectively infinite. This is also observed on Figures 9 and 10. In reality, ductile materials could keep deforming without yielding for a very long period of time or up to full closure of the tunnel.

Figure 9. (Left) Numerical results of LDPs for the drill and blast (DB) case of the BURGERS (B) analysis (the hours on the legend denote hours per excavation cycle), (Right) closer representation of the data for x values of -10 < X < 50.

Figure 10. (Left) Numerical results of LDPs for the TBM case of the BURGERS (B) analysis (the hours on the legend denote hours per excavation cycle), (Right) closer representation of the data for x values of -10 < X < 50.

In this part, it was noticed that the magnitude of the total displacements between the two cases varied significantly. The excavation method influences the accumulated displacements. In the drill and blast case, all three sets of models (parameters) exhibited less displacement than the TBM case for the same duration of the excavation cycles. During a tunnel excavation by a TBM, the tunnel excavation requires more time than a drill and blast excavation for the same excavation cycle. For instance, a TBM that excavates 1 m every 6 hours the elapsed time is three times longer than the drill and blast case of 3 m excavation per cycle. As a result, the time for the excavation of the same length tunnel will result in accumulation of displacement increase in the case of the TBM. However, in reality this may not always represent real conditions as TBMs are commonly preferable since they tend to achieve better excavation rates; if the rock mass conditions and the tunnel length make TBMs affordable. If the latter is the case, then a TBM excavation (Figure 10) of a two-hour excavation cycle, it is shown that the surrounding rock mass represented by SET#1 exhibits less displacement than of an eight-hour excavation cycle using drill and blast (Figure 9).

5 DISCUSSION

Another aspect of this study was to analyze the boundary and model conditions when creep behaviour manifests. Figures 11 and 12 show the stress-paths related to the numerical analyses presented herein for both cases drill and blast and TBM, where σ_{zz} and σ_{xx} are the major and minor stresses in the model, p is the mean stress and q the deviatoric, x refers to the location in the tunnel and R is the tunnel radius. Creep in these models is in response to differential stress (represented by q in the following figures) while the confining pressure (p) acts to resist yield but not creep in the visco-elastic case modelled here.

It is shown that the excavation step influences the stress regime in the tunnel. In the TBM case, where the excavation step is 1 m per excavation cycle, the stresses redistribute in a different manner than with the Drill and Blast case (3 m per cycle). In theory, the deviatoric stress (q) in both cases should reach the in situ pressure, p (as the radial stresses are zero and tangential stresses are 2p at the boundary). This does not occur in the model as the stresses are averaged in the grid zones. The deviatoric stress would approach the value of in situ stress if the elements in the numerical mesh were very small.

Figure 11. Stress paths for the drill and blast case.

Figure 12. Stress paths for the TBM case.

For a better understanding of the results the deviatoric stress was related to the displacement data normalized to the maximum displacement of the Kelvin-Voigt model ($u_r{}^{\infty}{}_{max}$). Only the results from the KELVIN-VOIGT analysis are presented and related to the deviatoric stress as it was noticed that time-dependent behaviour initiates at the same stress level and from the same location for all three sets and are shown in Figures 13 and 14 for the drill and blast case and the TBM, respectively; where: x is the distance from the tunnel face, R is the tunnel radius, u_r is the radial tunnel wall displacement, $u_r e_{max}$, q_{cr} denotes the deviatoric stress at which creep initiates.

Figure 13. (Left) Relating the deviatoric stress (q) to the tunnel wall displacement normalized to the maximum displacement of the KELVIN-VOIGT model ($u_r{}^{\infty}{}_{max}$) for the drill and blast case (D&B), (Right) closer representation of the data for x values of $-6 < X < 12$.

Figure 14. (Left) Relating the deviatoric stress (q) to the tunnel wall displacement normalized to the maximum displacement of the KELVIN-VOIGT model ($u_r{}^{\infty}{}_{max}$) for the TBM case, (Right) closer representation of the data for x values of $-2 < X < 4$.

Time-dependent behaviour starts for both cases and all data sets when the deviatoric stress reaches a critical value (q_{cr}) shown in Figures 13 and 14. This critical value is attained after one excavation step. In the drill and blast case, this is 3 m away from the tunnel whereas for the TBM case it is 1 m. It is at the point at which the time-dependent LDPs deviate from the elastic LDP. Until this critical point, the rock mass behaves elastically.

Implications during the tunnel construction may arise due to time-dependent deformation. Figure 15 shows the radial displacement of chainage at 1444 m of Saint Martin La Porte tunnel that exhibited severe squeezing and creep behaviour (Barla, 2016). It is illustrated that the rock mass deformed 60 cm during a period of 166 days. A schematic representation of the possible LDPs is also presented herein.

Figure 15. Predicted LDPs according to the tunnel data of radial displacement against distance (modified after Barla, 2016).

6 CONCLUSIONS

Analytical solutions often utilized in Convergence-Confinement analyses usually examine either the effect of tunnel advancement or the time-effect. Even in the latter case where time is considered, as shown in Figure 16 (i.e. Panet, 1979 curves), the overall displacement can be estimated. As this could be partially used for the selection of the final support, one may wonder if it could also be possible to simulate and replicate the complete problem. In this regard, an overview of the conventional methods used to predict the Longitudinal Displacement Profile of the radial displacements was presented and the limitations were highlighted. For this purpose, numerical analyses were performed where the displacement is both a function of time and the excavation advancement. More specifically, a parametric axisymmetric study was employed taking into consideration both effects (tunnel advancement and time) where three sets of models with different visco-elastic parameters were investigated under different conditions. It was shown that the effect of only the primary creep can lead to even 50% increase of the initial displacement and that the creep-parameters control the time the displacement will reach a constant value. There is no theoretical bound (other than full closure) when considering secondary creep. This could be the case of ductile rocks and rock masses like salt. The excavation method also controls the overall displacement as discussed. Different results may assist the selection of utilizing drill and blast over a TBM excavation if it is proven to be financially affordable. Finally, tunnel data were presented where time-dependent deformations were exhibited, relative findings to this study were derived.

Figure 16. (Left) LDPs for the drill and blast (DB) and TBM case of the KELVIN-VOIGT (KV) analysis related to the analytical solutions (continued lines related to hours on the legend denote hours per excavation cycle), (Right) closer representation of the data for x values of $-5 < X < 15$.

In regards to time-dependent deformation taking place in an underground environment it would contribute to both science and practice if a complete tunnel dataset was utilized with monitoring data and laboratory data in a numerical back-analysis. Especially in some cases, it is valuable to attain data acquired over years of monitoring to be able to capture the full rock mass response as for example, in the case of creep behaviour where also the contribution of the support system could be further analyzed.

Being able to predict and estimate the rock mass response due to one excavation method versus another can lead to project optimization. Optimization of the design usually involves the appropriate selection of the excavation method and the support system that would allow the rock mass to further deform over time avoiding overstressing that could otherwise lead to support yielding and abrupt rock mass instabilities, safety issues and cost overruns (Paraskevopoulou and Benardos). It is encouraged thus, to further examine the geological model, its rheological behaviour potential and utilizing all data and information available that will improve the design of the overall project.

ACKNOWLEDGEMENTS

The authors would like to acknowledge funding for this research from the Nuclear Waste Management Organization of Canada (NWMO) and the Natural Sciences and Engineering Research Council of Canada (NSERC).

REFERENCES

Alejano, L.R., Rodríguez-Dono, A., Alonso, E., Fdez-Manín, G., 2009. Ground reaction curves for tunnels excavated in different quality rock masses showing several types of post-failure behavior, Tunneling and Underground Space Technology, 24 (6), 689–705

Aristorenas, G. 1992. Time-dependent behaviour of tunnels excavated in shale. Ph.D. Thesis, MIT.

Aydan, O., Akagi, T., and Kawamoto, T. 1996. The squeezing potential of rock around tunnels: theory and prediction with examples taken from Japan. J. Rock Mech. Rock Eng., 29 (3), 125-143.

Barla, G. 2001. Tunnelling under squeezing rock conditions. In: Kolymbas D (eds.) Tunnellingmechanics. Eurosummer-School, Innsbruck, 98 pages.

Barla, G., Bonini, M., and Debernardi, D. 2010. Time-dependent Deformations in Squeezing Tunnels. International Journal of Geoengineering Case Histories, 2 (1), 819-824.

Barla, G. 2016. Full-face excavation of large tunnels in difficult conditions. Journal of Rock Mech and Geot Engin, 8(3), 294-303.

Brown E.T., Bray J.W., Ladanyi B., and Hoek, E., 1983. Ground response curves for rock tunnels. ASCE Journal of Geotechnical Engineering, 109(1): 15–39.

Cai Y., Yujing Jiang, Ibrahim Djamaluddin, Tomomi Iura, Tetsuro Esaki, 2015. An analytical model considering interaction behavior of grouted rock bolts for convergence–confinement method in tunneling design, International Journal of Rock Mechanics and Mining Sciences, Volume 76, 112-126.

Carranza-Torres, C., and Fairhurst, C. 2000. Application of the convergence-confinement method of tunnel design to rock masses that satisfy the Hoek-Brown failure criteria. Tunnelling and underground space Technology,15 (2), 187-213.

Chen, G. and Chugh, Y. 1996. Estimation of in situ visco-elastic parameter of weak floor strata by plate-loading tests. J. Geot. and Geol. Eng., 14 (2), 151-167.

Chern J.C, Shiao F.Y. and Yu C.W., 1998. An empirical safety criterion for tunnel construction. In: Proc. of the Regional Symposium on Sedimentary Rock Engineering, Taipei, Taiwan, 222–227.

Chin H.P. and Rogers, D.J. 1987. Creep parameters of rocks on an engineering scale. Rock Mechanics and Rock Engineering, 20, 137 – 146.

Corbetta, F., Bernaud, D., and Nguyen-Minh, D. 1991. Contribution a la methode convergence–confinement par le principle de la similitude. Rev. Fr. Geotech. 54, 5–11.

Lan Cui, Jun-Jie Zheng, Rong-Jun Zhang, Han-Jiang Lai, 2015. A numerical procedure for the fictitious support pressure in the application of the convergence–confinement method for circular tunnel design, International Journal of Rock Mechanics and Mining Sciences, 78, 336-349.

Damjanac, B., and Fairhurst, C. 2010. Evidence for a long-term strength threshold in crystalline rock. Rock Mech. Rock Eng., 43 (5), 513-531.

Debernardi, D. 2008. Visco-plastic behaviour and design of tunnels. Ph. D. Thesis, Politecnico di Torino, Italy.

Duncan-Fam, M.E. 1993. Numerical modelling of yield zones in weak rocks. In: Hudson, J. A. (ed.), Comprehensive Rock Engineering, Pergamon Press, Oxford, 2, 49-75.

Fahimifar, A., Monshizadeh Tehrani, F., Hedayat, A., and Vakilzadeh, A. 2010. Analytical solution for the excavation of circular tunnels in a visco-elastic Burgers material under hydrostatic stress field, Tunnel. Underg. Space Technol. doi: 10.1016/j.tust.2010.01.002.

Feng, X.T., Chen, B.R., Yang, C., X., and Zhiou, H. 2006. Intelligent analysis of rheological characteristic of rock materials. In: Proc. of Multiphysics coupling and long-term behaviour of rock mechanics, 275-280.

Fenner, R. 1938. Untersuchungen zur Erkenntis des Gebirgsdruckes bluckauf. 74, 671-695, 705-715.

Gnirk P.F., and Johnson R.E. 1964. The deformational behaviour of a circular mine shaft situated in a visco-elastic medium under hydrostatic stress. In: Proc. of the 6th symposium on rock mechanics, University of Missouri (Rolla), 231–259.

González-Cao J., F. Varas, F.G. Bastante, L.R. Alejano, 2013. Ground reaction curves for circular excavations in non-homogeneous, axisymmetric strain-softening rock masses, Journal of Rock Mechanics and Geotechnical Engineering, 5(6), 431–442.

Goodman, R.E. 1980. Introduction to Rock Mechanics, John Wiley and Sons, New York.

Gschwandtner, G.G., and Galler, R., 2012. Input to the application of the convergence confinement method with time-dependent material behaviour of the support, Tunnelling and Underground Space Technology, 27(1), 13-22.

Itasca. 2011. FLAC. Version 7. User’s manual. 2D Version. Available at [www.Itascacg.com].

Kalos, A. 2014. Investigation of the nonlinear time-dependent soil behaviour, Ph.D. Thesis, National Technical University of Athens, Greece.

Kontogianni, V., Psimoulis, P., and Stiros, S. 2005. What is the contribution of time-dependent deformation in tunnel convergence? Engineering Geology, 82, 264– 267.

Lama, R.D. and Vutukuri, V.S. 1978. Mechanical properties of rocks, 3. Trans Tech, Rock port, MA.

Lo, K.Y. and Yuen, C.M.K. 1981. Design of tunnel lining in rock for long-term time effects. Can Geotech. Journal., 18, 24-39.

Lockner, D. 1993. Room temperature creep in saturated granite. J. Geophys. Res. 98, 475–487.

Lombardi, G., 1975. Qualche aspetto particolare della statica delle cavita sotterranee. Rivista Italiana di Geotecnica, 2, 187-206.

Malan, D.F., Vogler, U.W., and Drescher, K. 1997. Time-dependent behaviour of hard rock in deep level gold mines. J. S. Afr. Inst. Min. Metall., 97, 135-147.

Mirza, U.A. 1978. Investigation into the design criteria for underground openings in rocks which exhibit rheological behaviour. Ph.D. Thesis, University of Newcastle-upon-Tyme, UK.

Nomikos, P., Rahmannejad, R., and Sofianos, A. 2011. Supported axisymmetric tunnels within linear visco-elastic Burgers rocks. Rock Mechanics and Rock Engineering, 44 (5), 553–564.

Pan Y.W., and Dong, J.J. 1991. Time-dependent Tunnel Convergence II. Advance Rate and Tunnel- Support Interaction. Int. J Rock Mech Min Sci Geomech, 28(6), 477–488

Panet, M. 1979. Time-dependent deformations in underground works. In: Proc. of the 4th Int Congress on Rock Mechanics, Montreux.

Panet, M., and Guenot, A. 1982. Analysis of convergence behind the face of a tunnel. In: Proc. of the International Symposium Tunnelling, IMM, London, 197–204.

Panet, M. 1993. Understanding deformations in tunnels. In: Hudson JA, Brown ET, Fairhurst C, Hoek E (eds) Proc. of the Comprehensive Rock Engineering, Vol. 1. Pergamon, London, 663–690.

Panet, M. 1995. Calcul des Tunnels par la Methode de Convergence–Confinement. Presses de l'Ecole Nationale des Ponts et Chausse'es, Paris, 178 pages.

Paraskevopoulou, C., and Benardos, A. 2013. Assessing the construction cost of tunnel projects. Tunnelling and Underground Space Technology, 38, 497-505.

Paraskevopoulou, C., and Diederichs, M.S. 2013. A comparison of viscous models under constant strain and constant stress: Implications for tunnel analysis. In: Proc. of the World Tunnel Congress, Geneva, Switzerland.

Paraskevopoulou, C. 2016. Time-dependency of rocks and implications associated with tunnelling. Ph.D. Thesis, Queen's University, Canada.

Parcher, F. 1964, Deformationsmessung in Versuchstollen als Mittel zur Erforeschung des Gebirgsverhaltens und zur Bemmessung des Ausbaues. Felsmechanik und Ingenieurgeologie Supplementun, IV, 149-61.

Peila, D., and Oreste P.P. 1995. Axisymmetric analysis on ground reinforcing in tunnelling design. Comput Geotech, 17, 253–274.

Perzyna, P. 1966. Fundamental problems in visco-plasticity. Advances in applied mechanics, 9 (2), 243-377.

Sakurai, S. 1978. Approximate time-dependent analysis of tunnel support structure considering progress of tunnel face. Int. J. Numer. Anal. Methods Geomech. 2, 159–175.

Singh, A.K., Balasingh, C., Mao, H-K., Hemley, R.J., and Shu, J. 1998. Analysis of lattice strains measured under nonhydrostatic pressure. J. Appl. Phys., 83, 7567-75.

Sterpi, D., and Gioda, G. 2009. Visco-plastic behaviour around advancing tunnels in squeezing rock. Rock Mech Rock Eng., 42, 319-339.

Sulem, J., Panet, M. and Guenot, A. 1987. Closure analysis in deep tunnels and Analytical solution for time-dependent displacement in a circular tunnel. Int. J. Rock Mech. & Min. Sci. & Geom. Abstracts. 24(3), 145-154 and 155-164.

Unlu, T, and Gercek H. 2003. Effect of Poisson's ratio on the normalized radial displacementsoccurring around the face of a circular tunnel. Tunn Undergr Sp Tech, 18, 547–553.

Vlachopoulos, N., Diederichs, M.S. 2009. Improved longitudinal displacement profiles for convergence confinement analysis of deep tunnels. Rock Mechanics and Rock Engineering. 42, 131-146.

Vrakas, A., 2017. A finite strain solution for the elastoplastic ground response curve in tunnelling: rocks with non-linear failure envelopes. International Journal for Numerical and Analytical Methods in Geomechanics, 41(7),1077-1190.

Vrakas, A. and Anagnostou, G., 2014. A finite strain closed-form solution for the elastoplastic ground response curve in tunnelling. International Journal for Numerical and Analytical Methods in Geomechanics, 38(11), 1131–1148.

Yiouta-Mitra, P., Sofianos, A.I., and Rahmannejad, R. 2010. Longitudinal deformation profile of a tunnel driven within a Burger rock mass. In Proc: of the ISRM International Symposium 2010 and 6th Asian Rock Mechanics Symposium - Advances in Rock Engineering, New Delhi, India.

Wang, S., Yin, X., Tang, H., Ge, X., 2010. A new approach for analyzing circular tunneling strain-softening rock masses, International Journal of Rock Mechanics& Mining Sciences,47, 170–178.

Zhang, H., Wang, Z., Zheng, Y., Duan, P., and Ding, S. 2012. Study on tri-axial creep experiment and constitutive relation of different rock salt. Safety Science, 50 (4), 801-5.

TABLE OF FIGURES

Figure 13. (Left) Relating the deviatoric stress (q) to the tunnel wall displacement normalized to the maximum displacement of the KELVIN-VOIGT model ($u_r\infty_{max)}$ for the drill and blast case (D&B), (Right) closer representation of the data for x values of -6 < X < 12.

Figure 14. (Left) Relating the deviatoric stress (q) to the tunnel wall displacement normalized to the maximum displacement of the KELVIN-VOIGT model ($u_r\infty_{max}$) for the TBM case, (Right) closer representation of the data for x values of -2 < X < 4.

Figure 15. Predicted LDPs according to the tunnel data of radial displacement against distance (modified after Barla, 2016).

Figure 16. (Left) LDPs for the drill and blast (DB) and TBM case of the KELVIN-VOIGT (KV) analysis related to the analytical solutions (continued lines related to hours on the legend denote hours per excavation cycle), (Right) closer representation of the data for x values of -5 < X < 15.

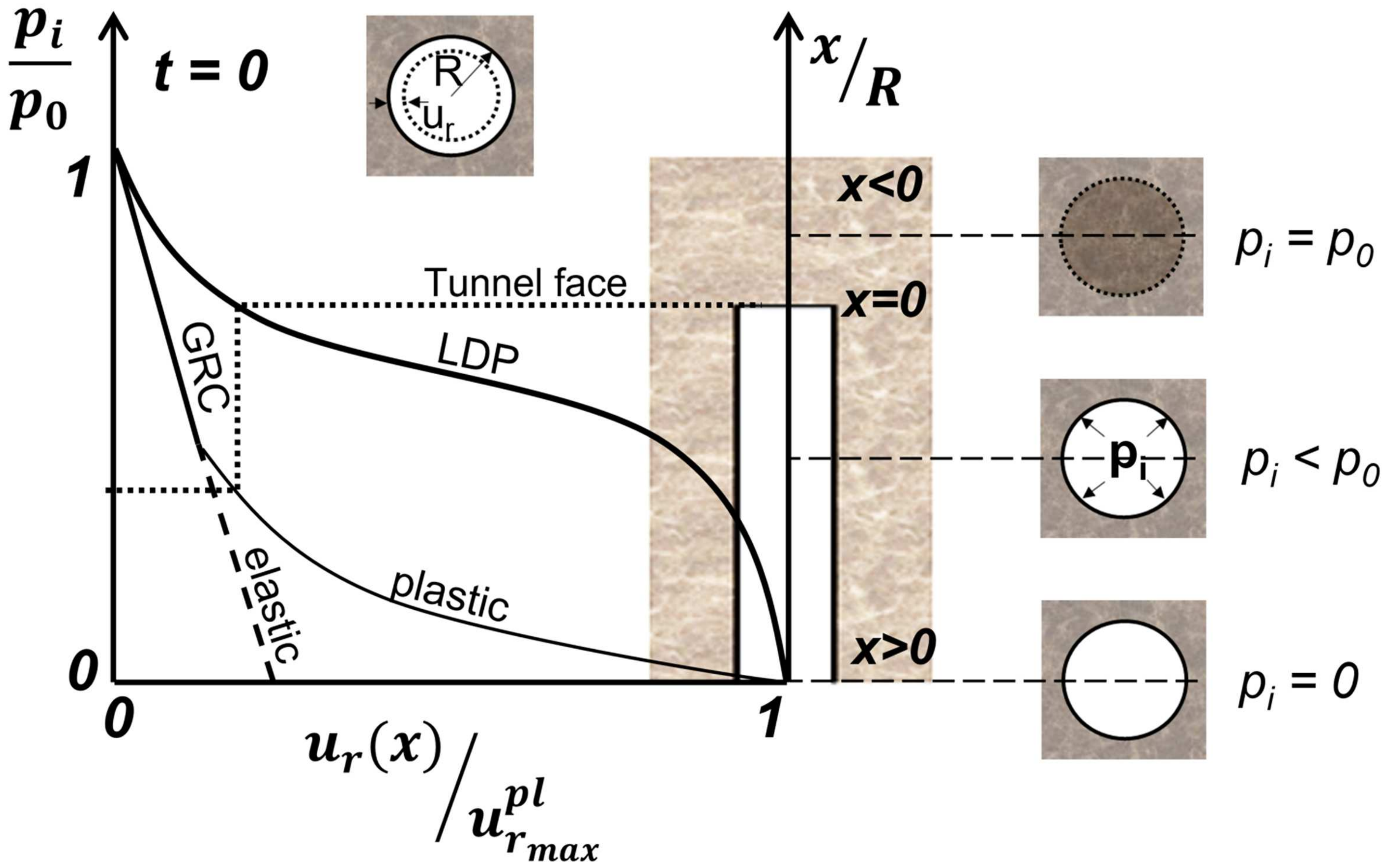

p_i / p_0
t = 0
R
u_r
x/R
1
x<0
$p_i = p_0$
Tunnel face
x=0
GRC
LDP
p_i
$p_i < p_0$
elastic
plastic
x>0
0
$p_i = 0$
0
1
$u_r(x) / u^{pl}_{r_{max}}$

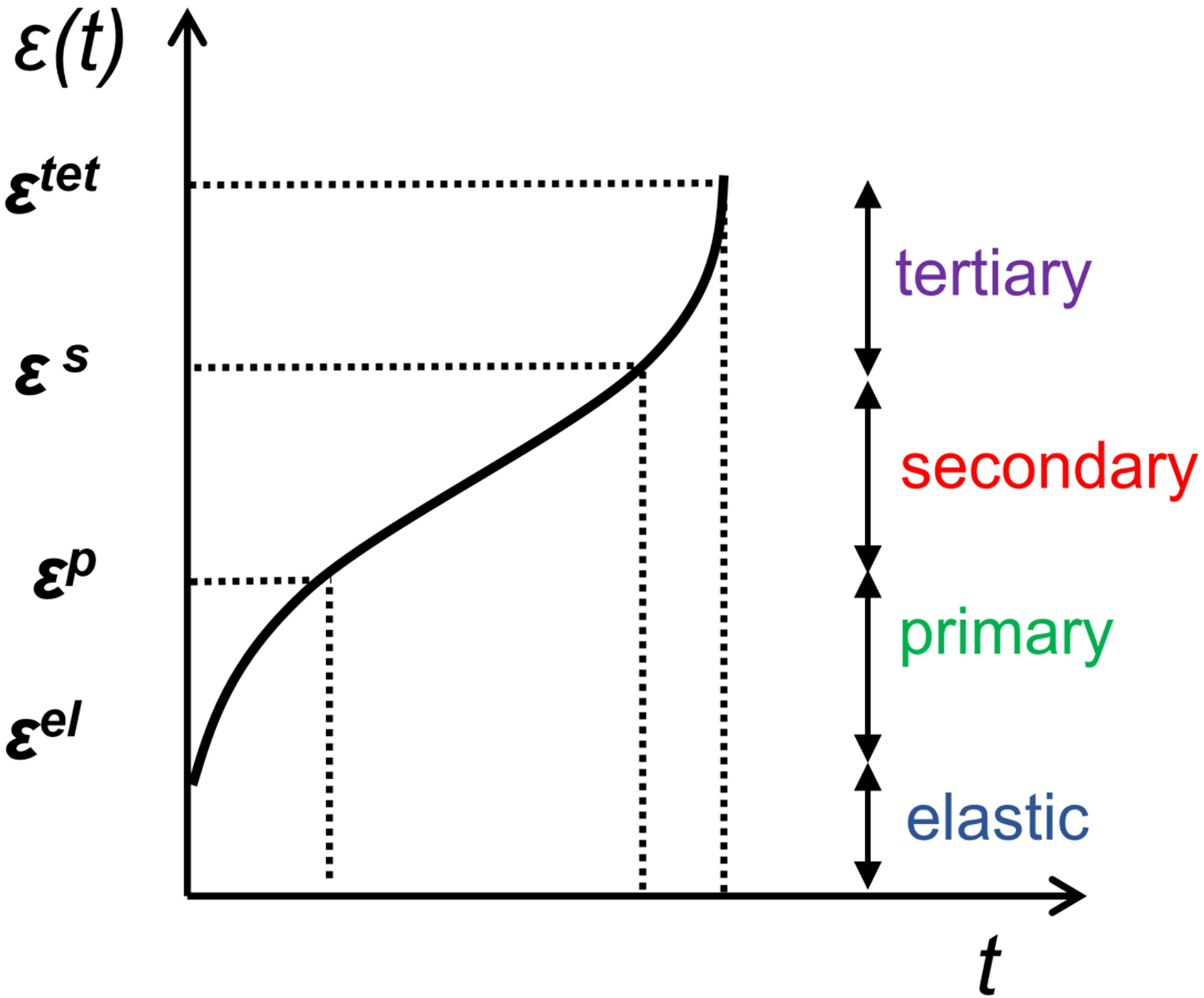

$\varepsilon(t)$
ε^{tet}
ε^{s}
ε^{p}
ε^{el}
tertiary
secondary
primary
elastic
t

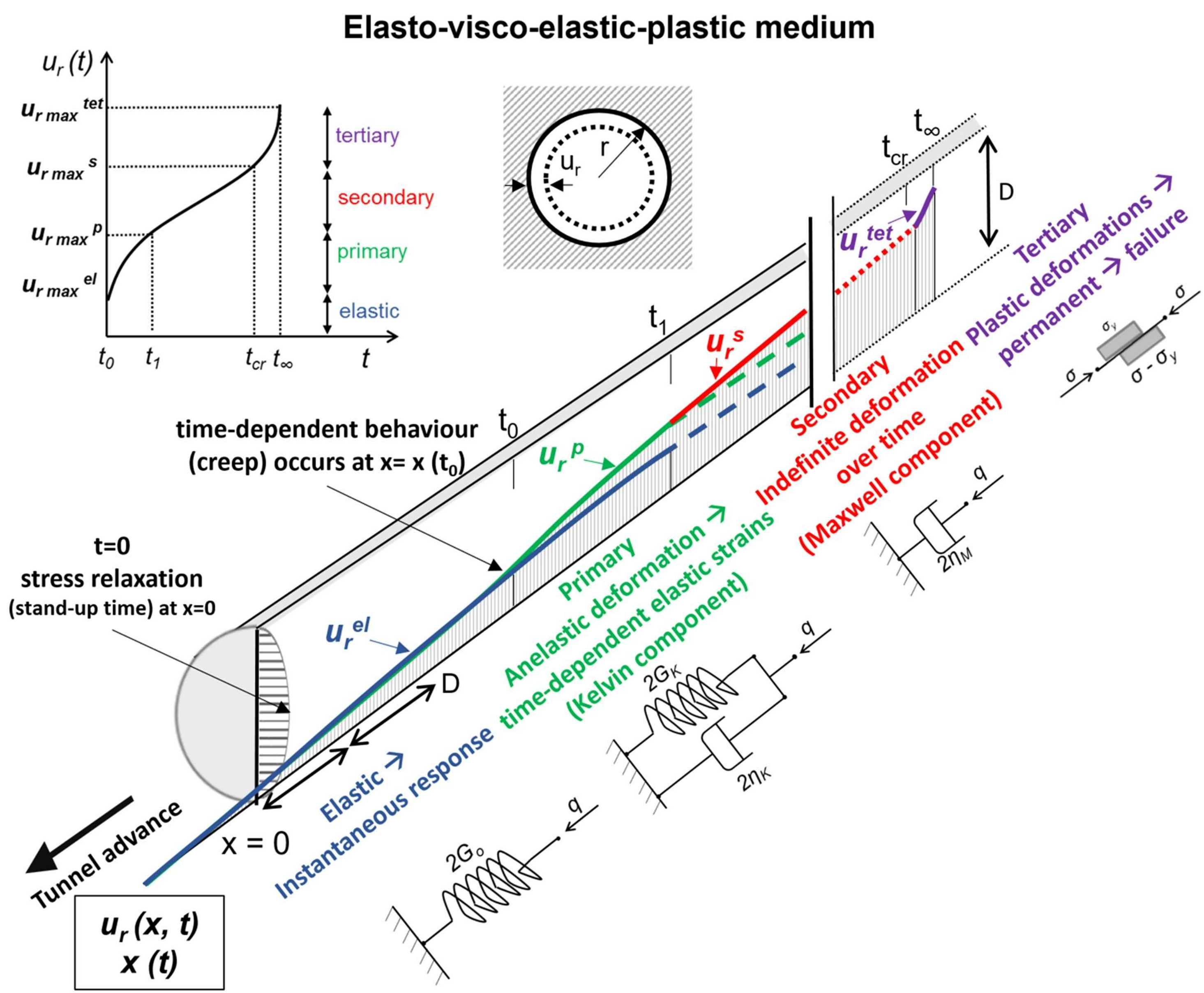

Elasto-visco-elastic-plastic medium
u_r (t)
u_r max^tet
u_r max^s
u_r max^p
u_r max^el
tertiary
secondary
primary
elastic
t_0 t_1 t_cr t_∞ t
u_r
r
t_∞
t_cr
D
u_r^tet
Tertiary
Plastic deformations →
permanent → failure
σ
σ_y
σ - σ_y
t_1
u_r^s
Secondary
Indefinite deformation
over time
(Maxwell component)
q
2η_M
time-dependent behaviour
(creep) occurs at x= x (t_0)
t_0
u_r^p
Primary
Anelastic deformation →
time-dependent elastic strains
(Kelvin component)
2G_K
2η_K
t=0
stress relaxation
(stand-up time) at x=0
u_r^el
D
Elastic →
Instantaneous response
2G_o
x = 0
Tunnel advance
u_r (x, t)
x (t)

Elasto-visco-elastic medium

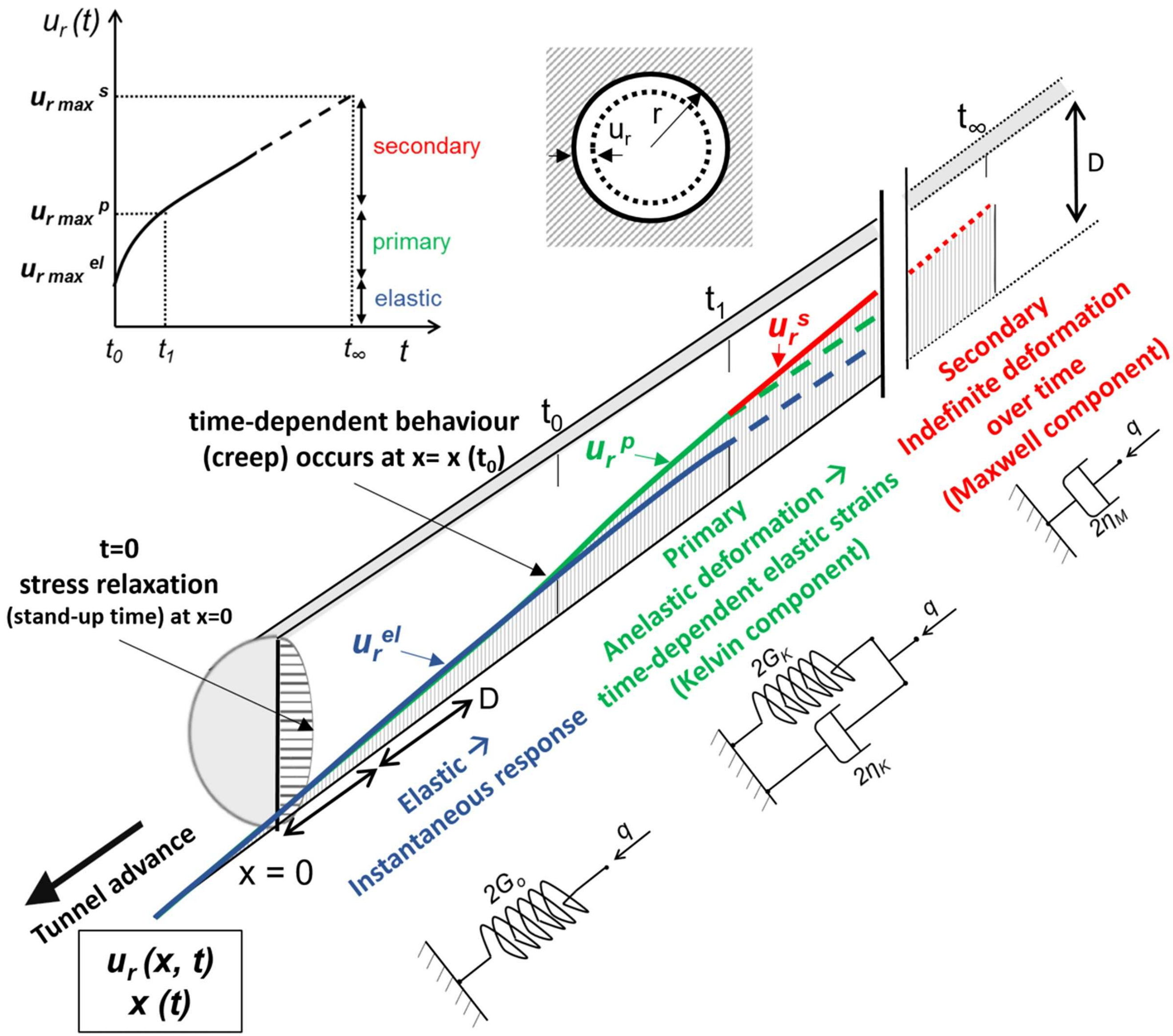

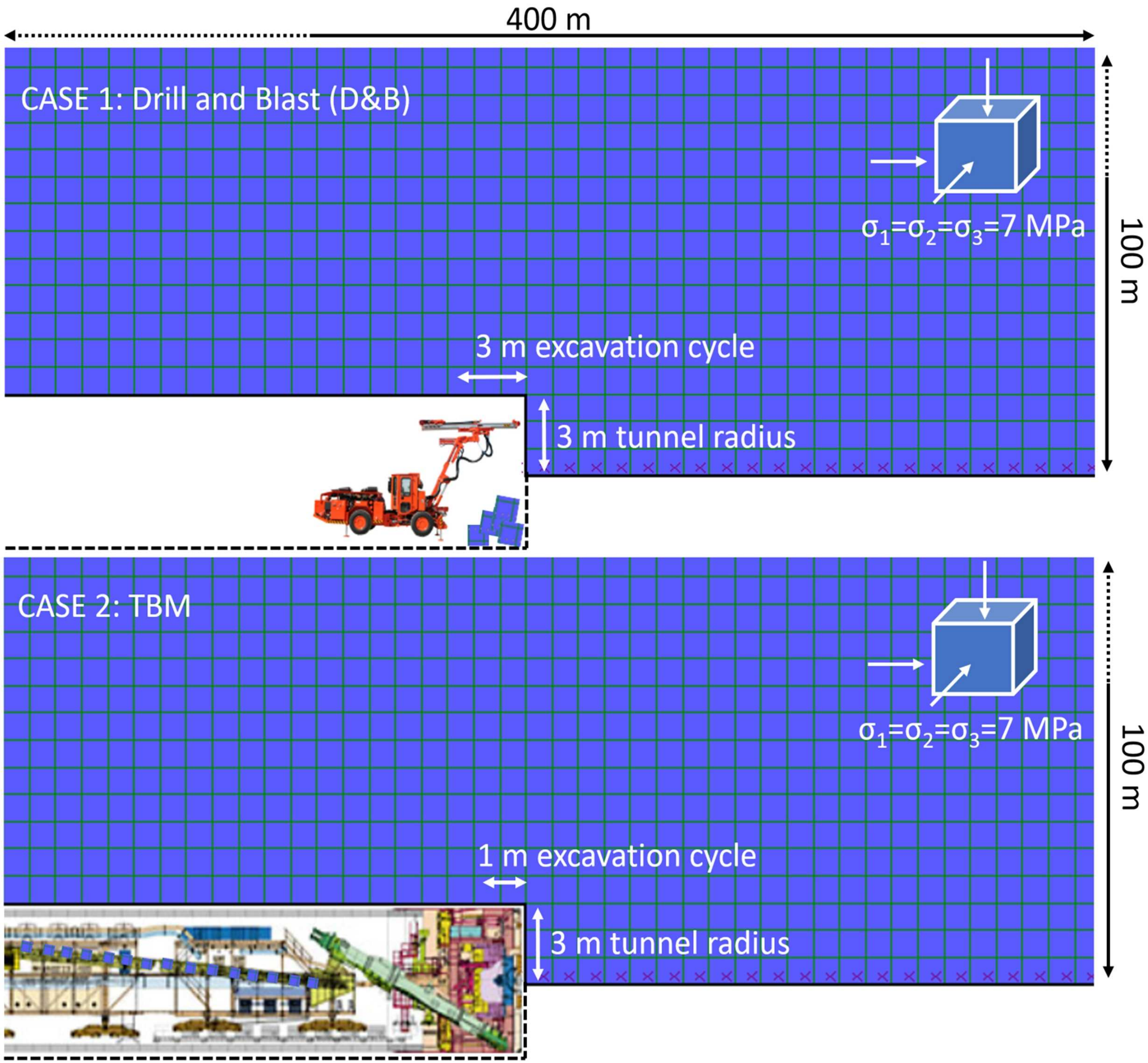

400 m
CASE 1: Drill and Blast (D&B)
σ1=σ2=σ3=7 MPa
100 m
3 m excavation cycle
3 m tunnel radius
CASE 2: TBM
σ1=σ2=σ3=7 MPa
100 m
1 m excavation cycle
3 m tunnel radius

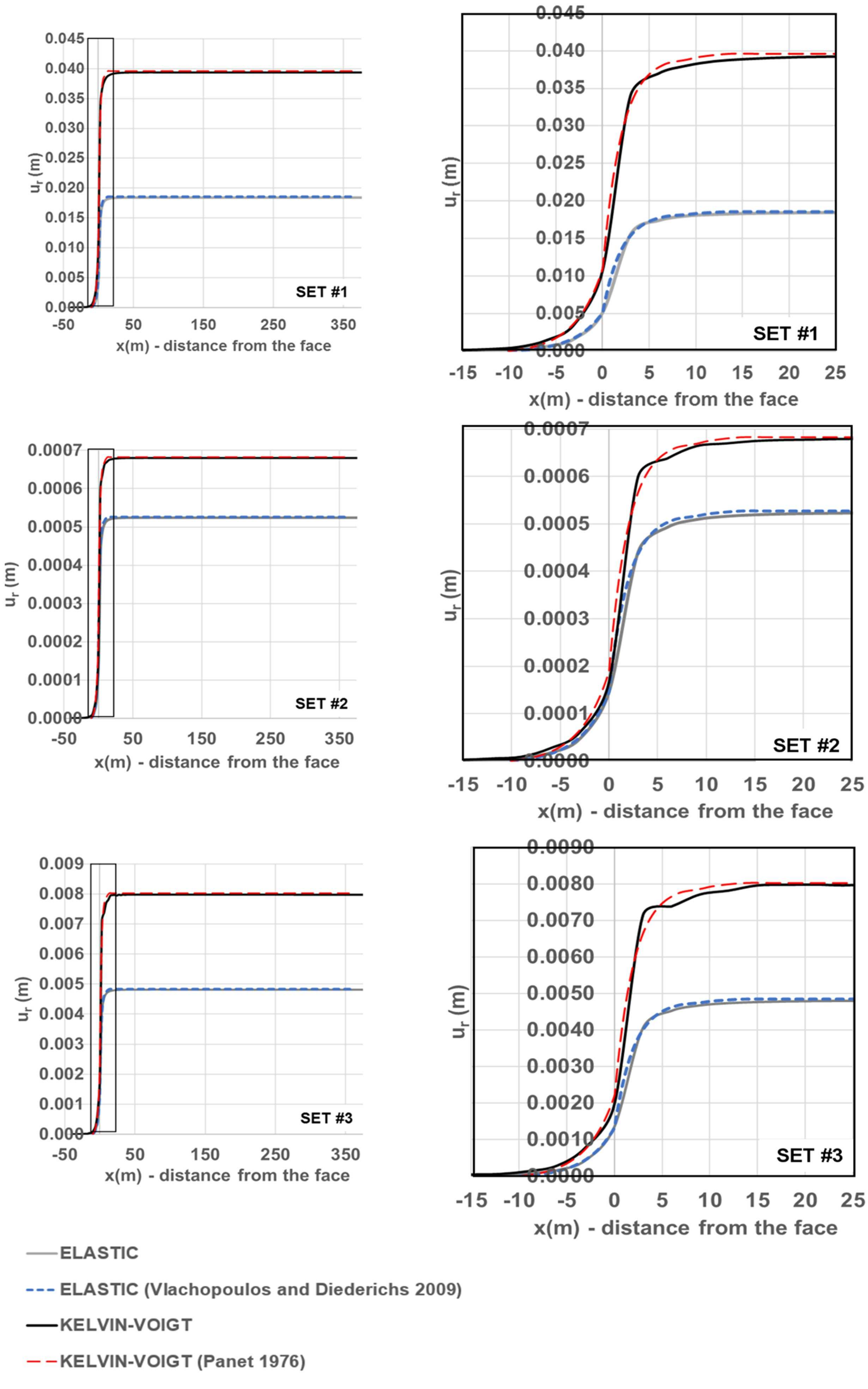
SET #1
SET #2
SET #3
u_r (m)
x(m) - distance from the face
ELASTIC
ELASTIC (Vlachopoulos and Diederichs 2009)
KELVIN-VOIGT
KELVIN-VOIGT (Panet 1976)

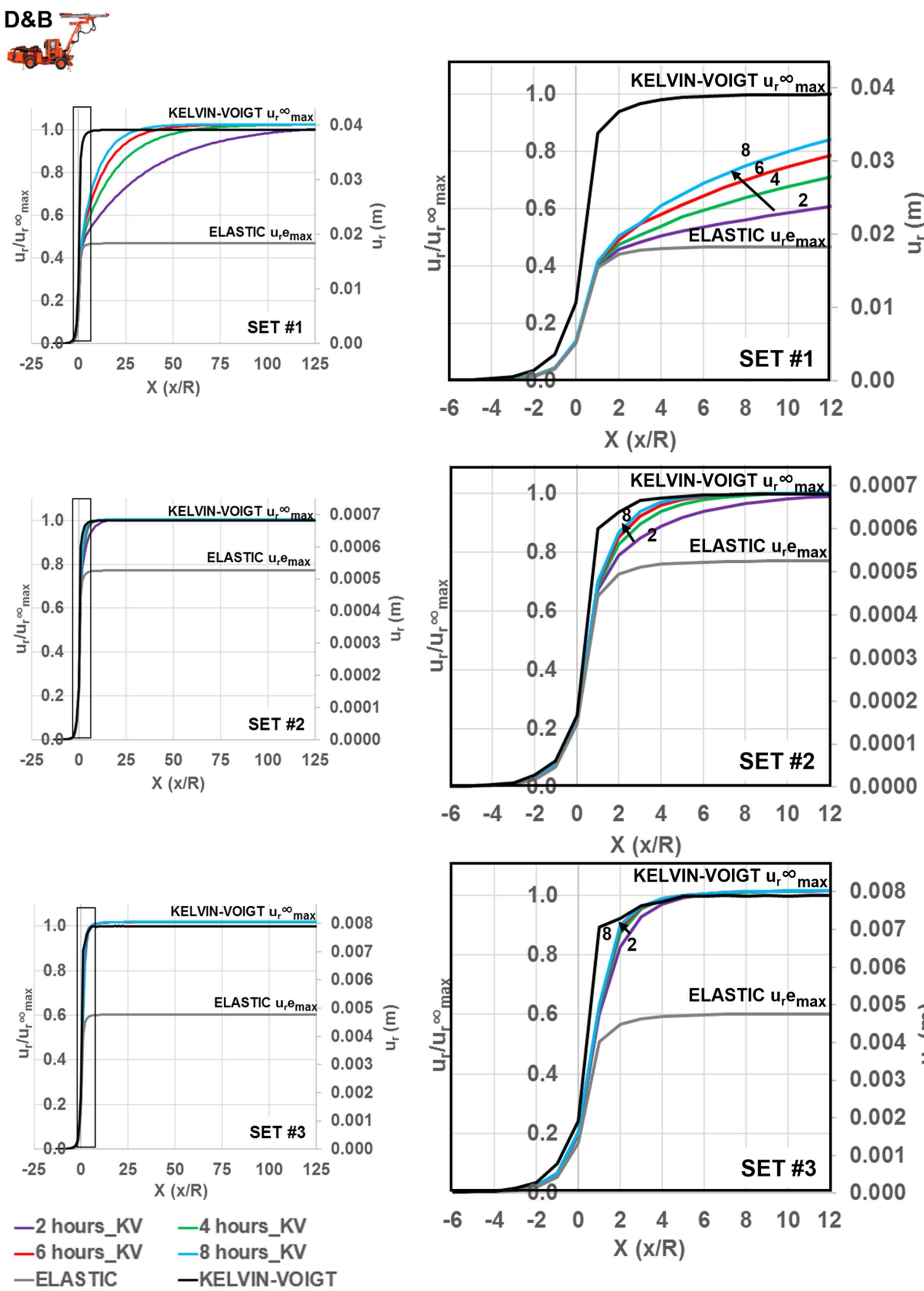
D&B
KELVIN-VOIGT $u_r\infty_{max}$
ELASTIC u_re_{max}
SET #1
SET #2
SET #3
$u_r/u_r\infty_{max}$
u_r (m)
X (x/R)
8
6
4
2
2 hours_KV
4 hours_KV
6 hours_KV
8 hours_KV
ELASTIC
KELVIN-VOIGT

TBM

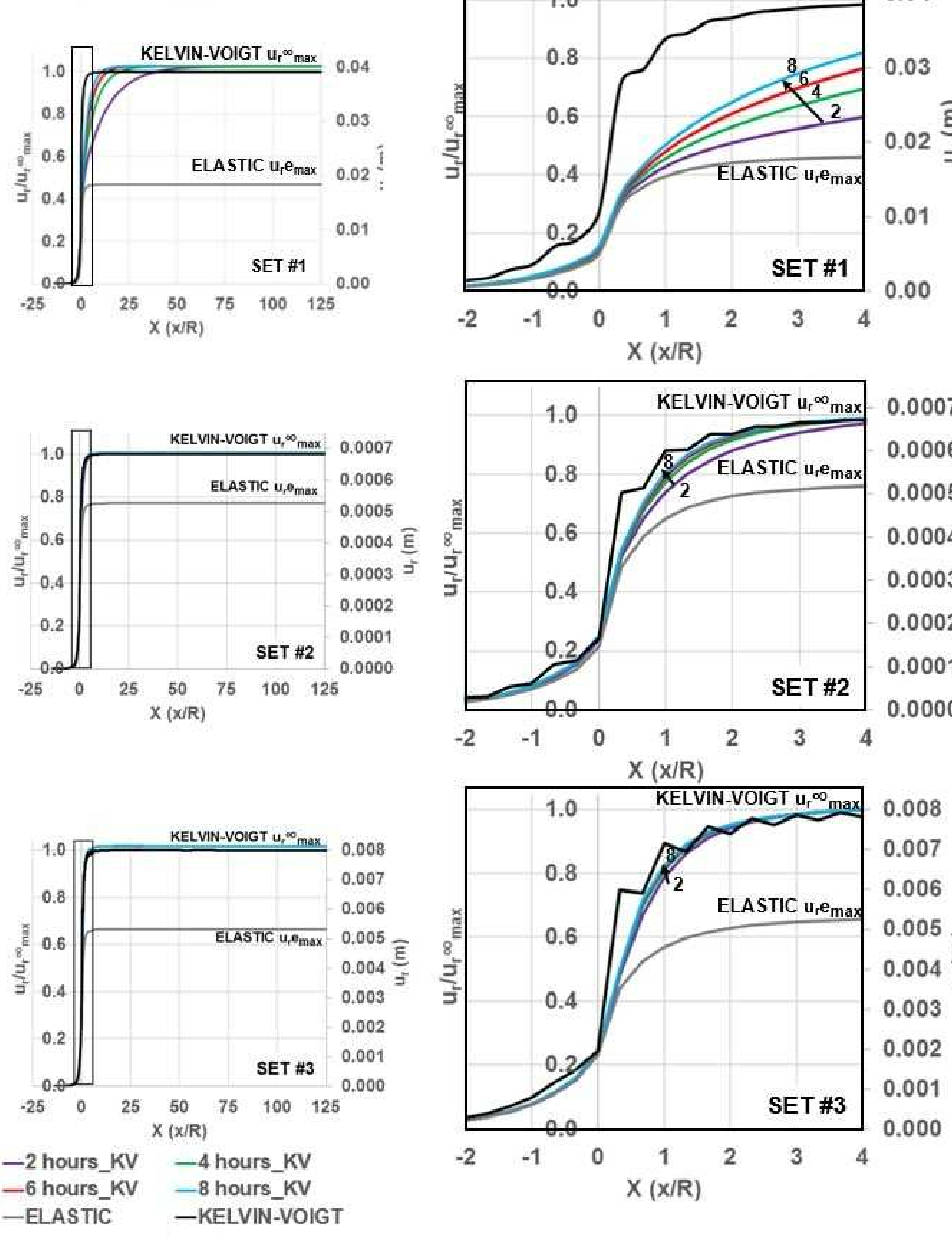
KELVIN-VOIGT $u_r^{\infty}{}_{max}$
ELASTIC $u_r e_{max}$
SET #1
SET #2
SET #3
$u_r/u_r^{\infty}{}_{max}$
u_r (m)
X (x/R)
2
4
6
8
2 hours_KV
4 hours_KV
6 hours_KV
8 hours_KV
ELASTIC
KELVIN-VOIGT

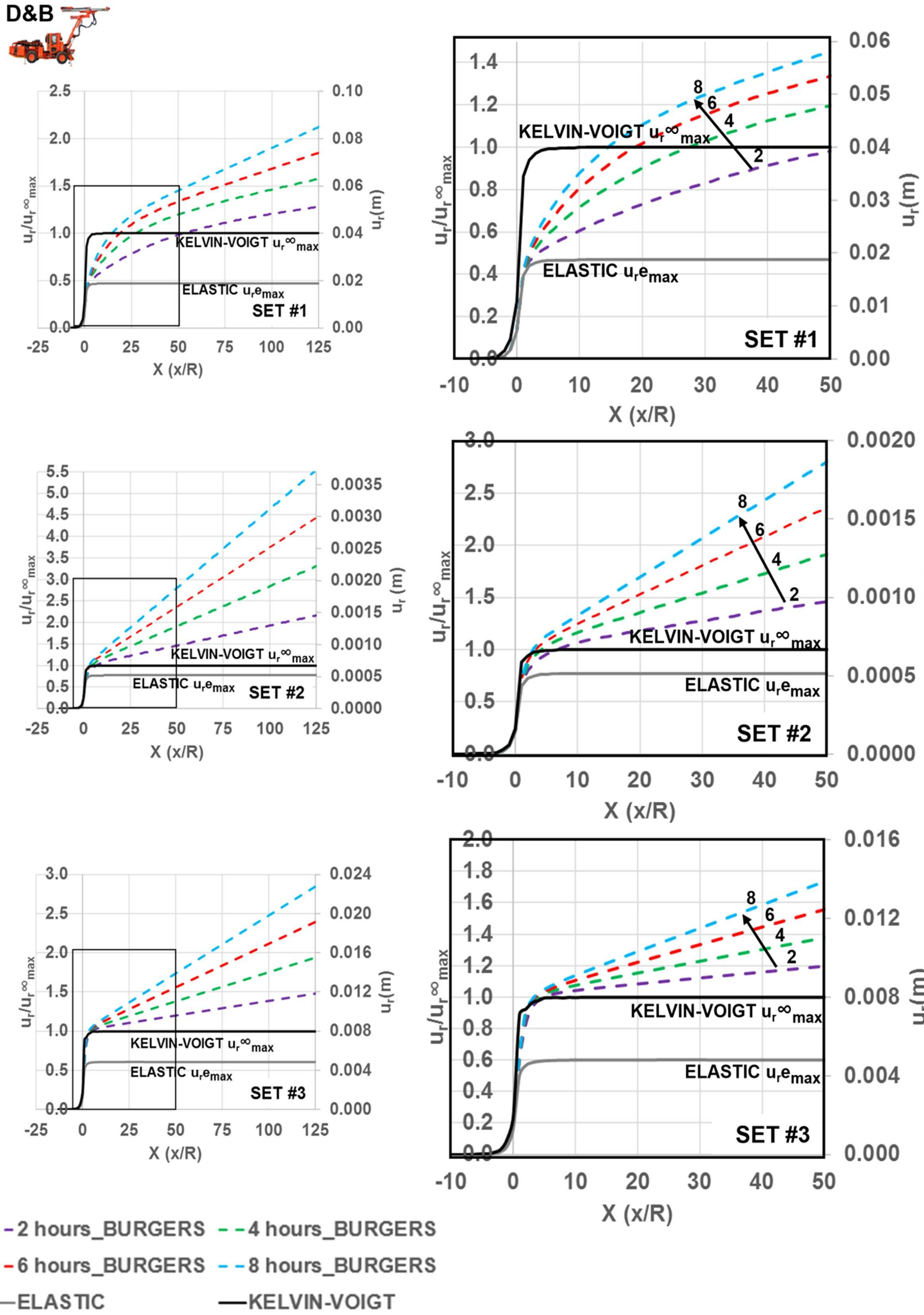
D&B
SET #1
SET #2
SET #3
KELVIN-VOIGT $u_r\infty_{max}$
ELASTIC $u_r e_{max}$
$u_r/u_r\infty_{max}$
u_r(m)
X (x/R)
8
6
4
2
2 hours_BURGERS
4 hours_BURGERS
6 hours_BURGERS
8 hours_BURGERS
ELASTIC
KELVIN-VOIGT

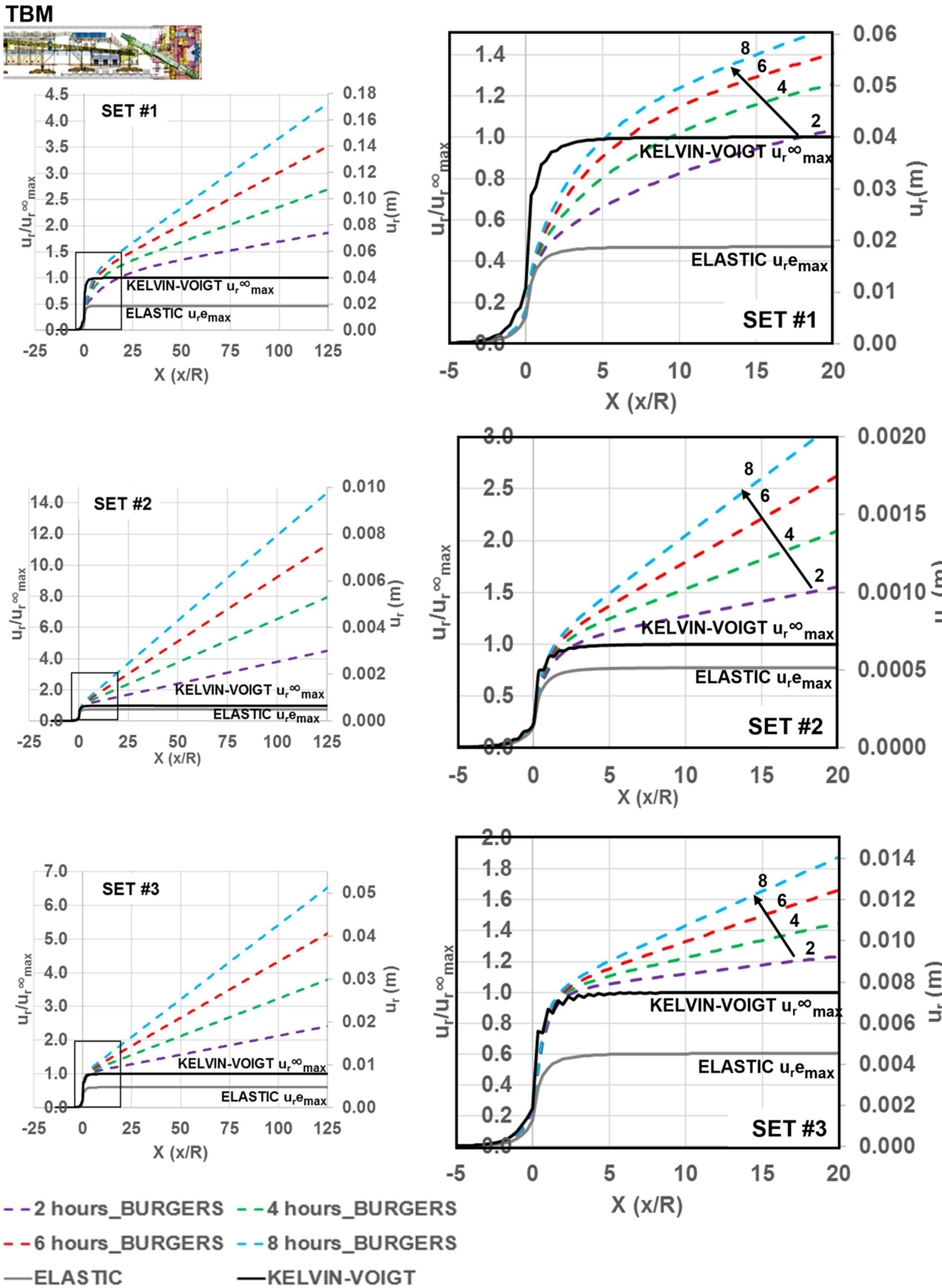

TBM
SET #1
SET #2
SET #3
KELVIN-VOIGT u_r∞_max
ELASTIC u_re_max
u_r/u_r∞_max
u_r (m)
X (x/R)
8
6
4
2
2 hours_BURGERS
4 hours_BURGERS
6 hours_BURGERS
8 hours_BURGERS
ELASTIC
KELVIN-VOIGT

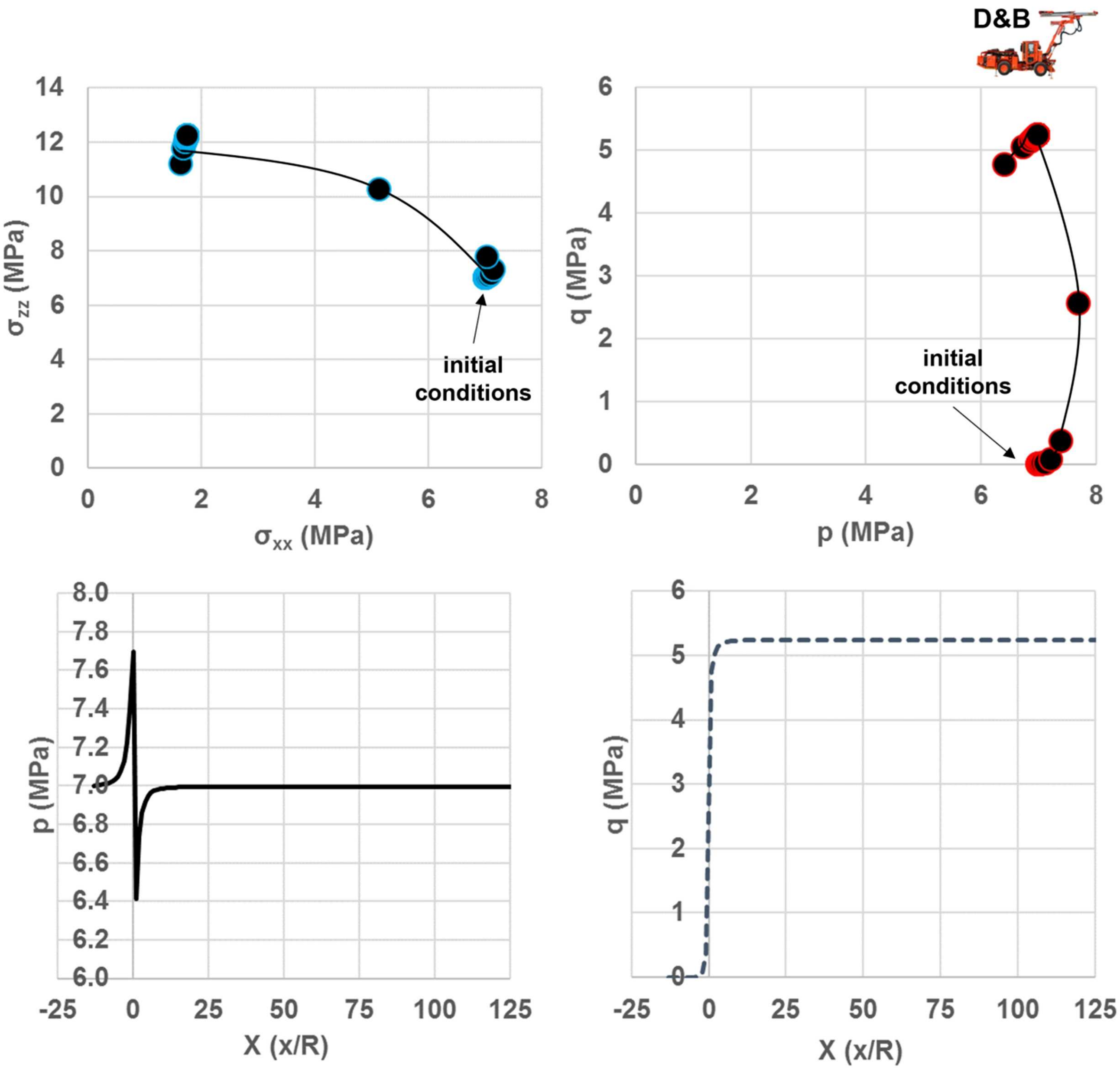
D&B
14
12
10
8
6
4
2
0
σ_{zz} (MPa)
0
2
4
6
8
σ_{xx} (MPa)
initial conditions
6
5
4
3
2
1
0
q (MPa)
0
2
4
6
8
p (MPa)
initial conditions
8.0
7.8
7.6
7.4
7.2
7.0
6.8
6.6
6.4
6.2
6.0
p (MPa)
-25
0
25
50
75
100
125
X (x/R)
6
5
4
3
2
1
0
q (MPa)
-25
0
25
50
75
100
125
X (x/R)

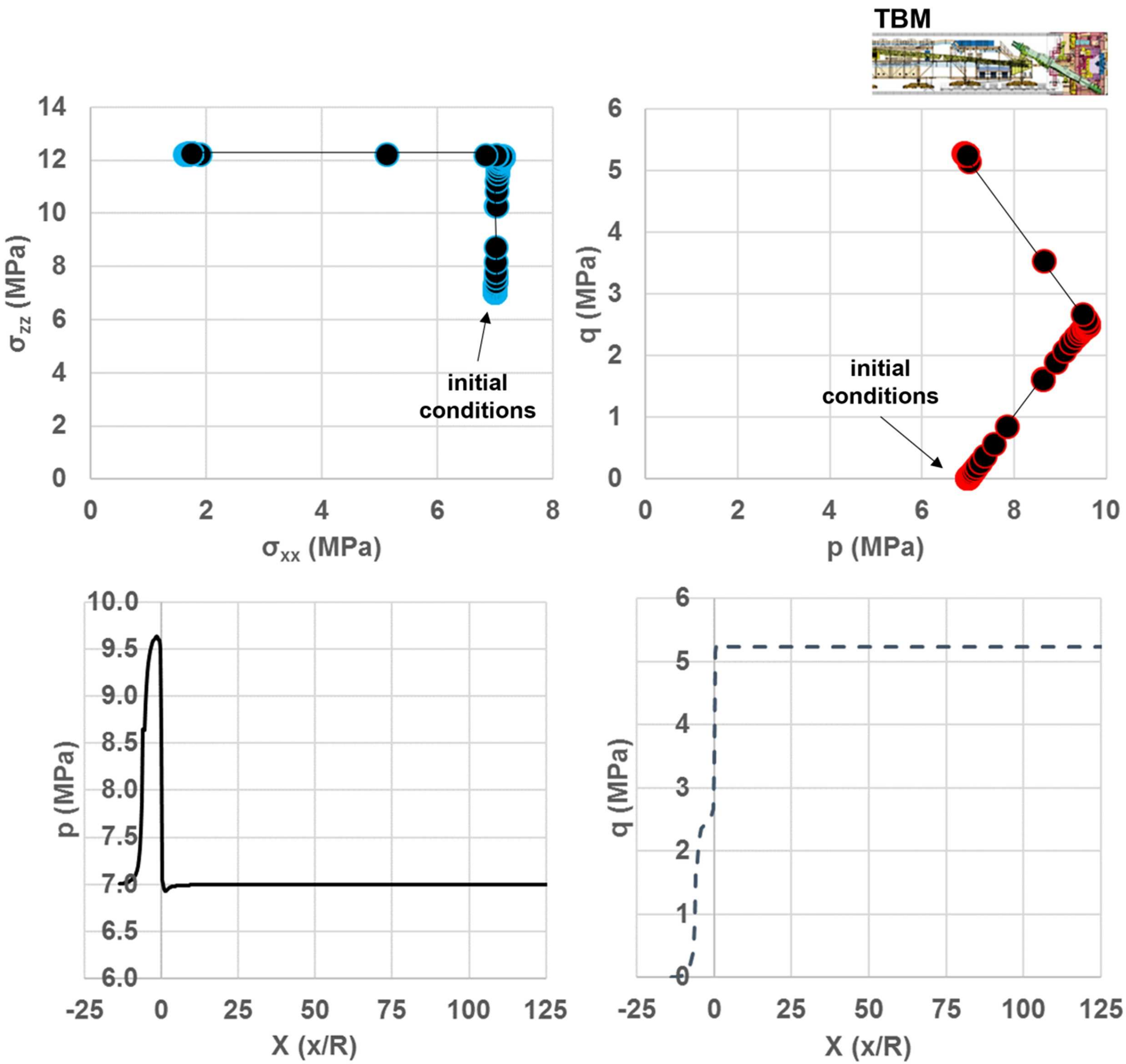

TBM
14
12
10
8
6
4
2
0
σzz (MPa)
initial conditions
0 2 4 6 8
σxx (MPa)
6
5
4
3
2
1
0
q (MPa)
initial conditions
0 2 4 6 8 10
p (MPa)
10.0
9.5
9.0
8.5
8.0
7.5
7.0
6.5
6.0
p (MPa)
-25 0 25 50 75 100 125
X (x/R)
6
5
4
3
2
1
0
q (MPa)
-25 0 25 50 75 100 125
X (x/R)

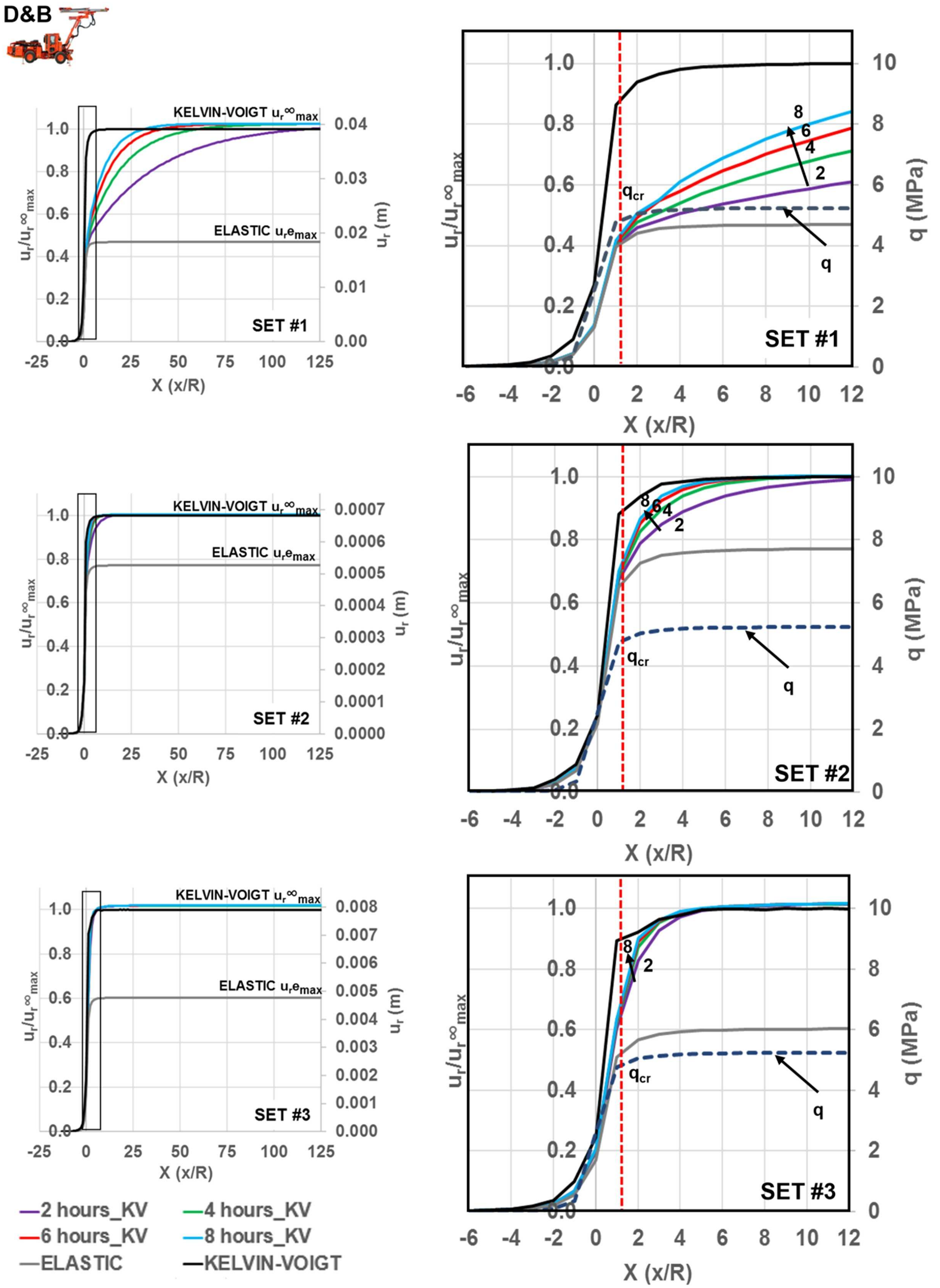

D&B
KELVIN-VOIGT $u_r\infty_{max}$
ELASTIC u_re_{max}
$u_r/u_r\infty_{max}$
u_r (m)
X (x/R)
q (MPa)
q_{cr}
q
SET #1
SET #2
SET #3
2 hours_KV
4 hours_KV
6 hours_KV
8 hours_KV
ELASTIC
KELVIN-VOIGT

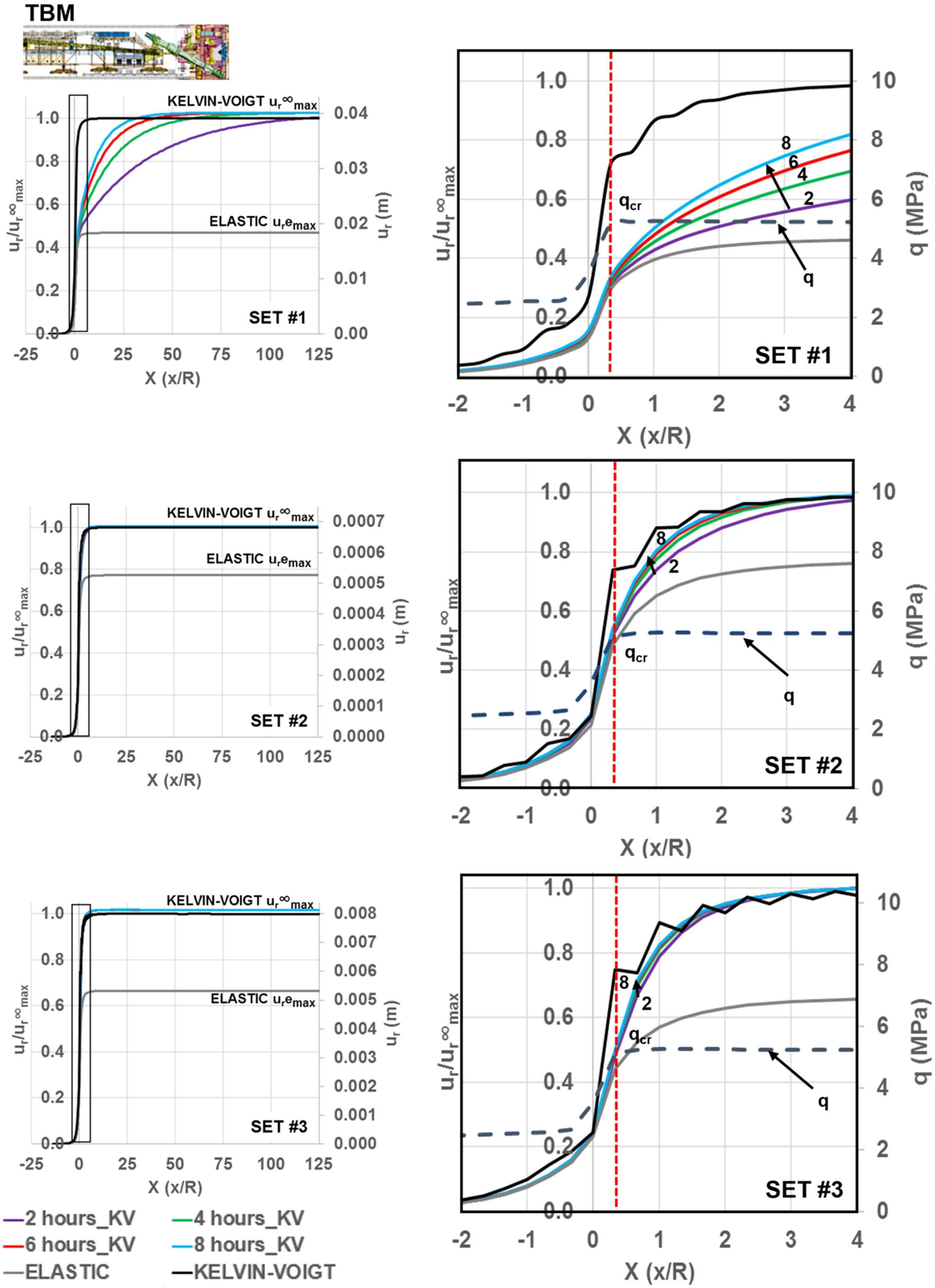

TBM
KELVIN-VOIGT $u_r^\infty{}_{max}$
ELASTIC $u_r e_{max}$
SET #1
SET #2
SET #3
q_{cr}
q
X (x/R)
$u_r/u_r^\infty{}_{max}$
u_r (m)
q (MPa)
2 hours_KV
4 hours_KV
6 hours_KV
8 hours_KV
ELASTIC
KELVIN-VOIGT

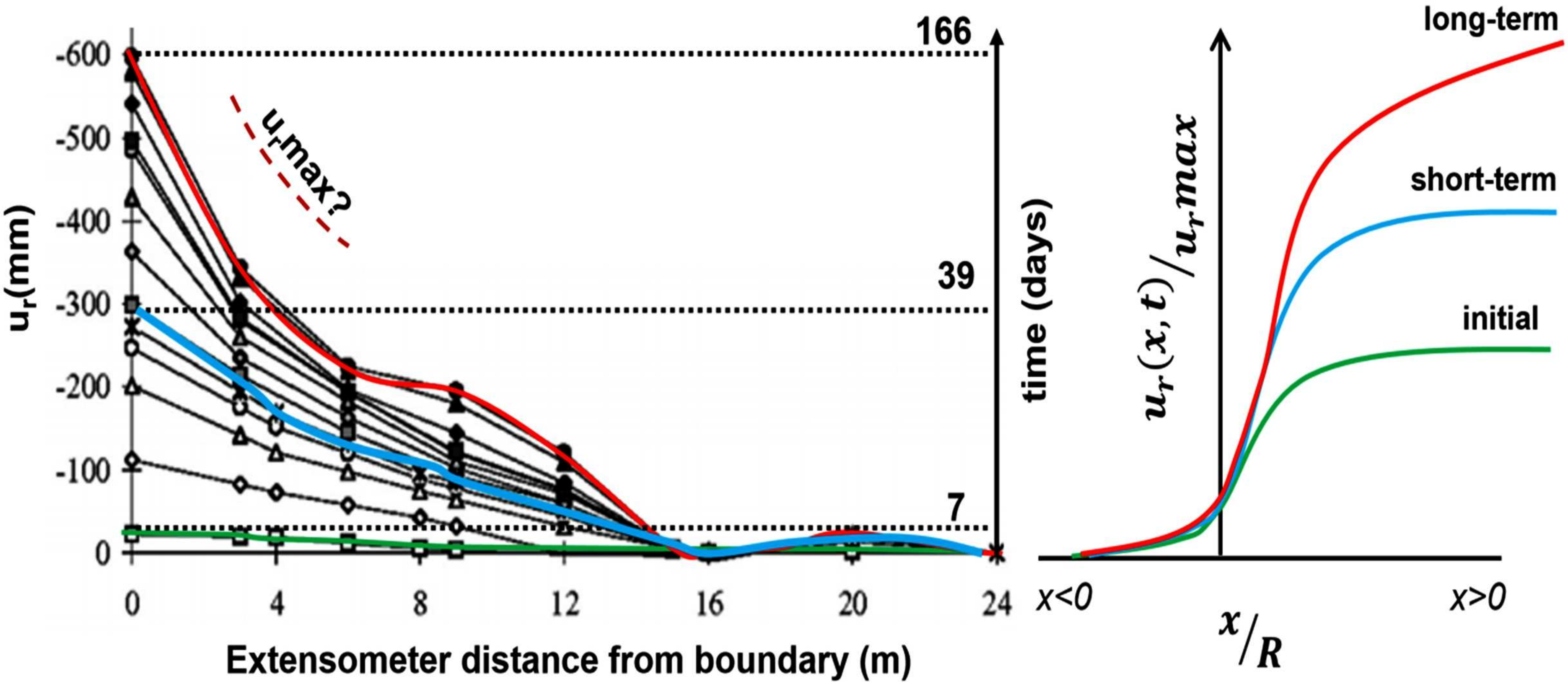

-600
-500
-400
-300
-200
-100
0
u_r(mm)
u_rmax?
166
39
7
time (days)
0
4
8
12
16
20
24
Extensometer distance from boundary (m)
long-term
short-term
initial
$u_r(x,t)/u_r max$
x<0
x>0
x/R

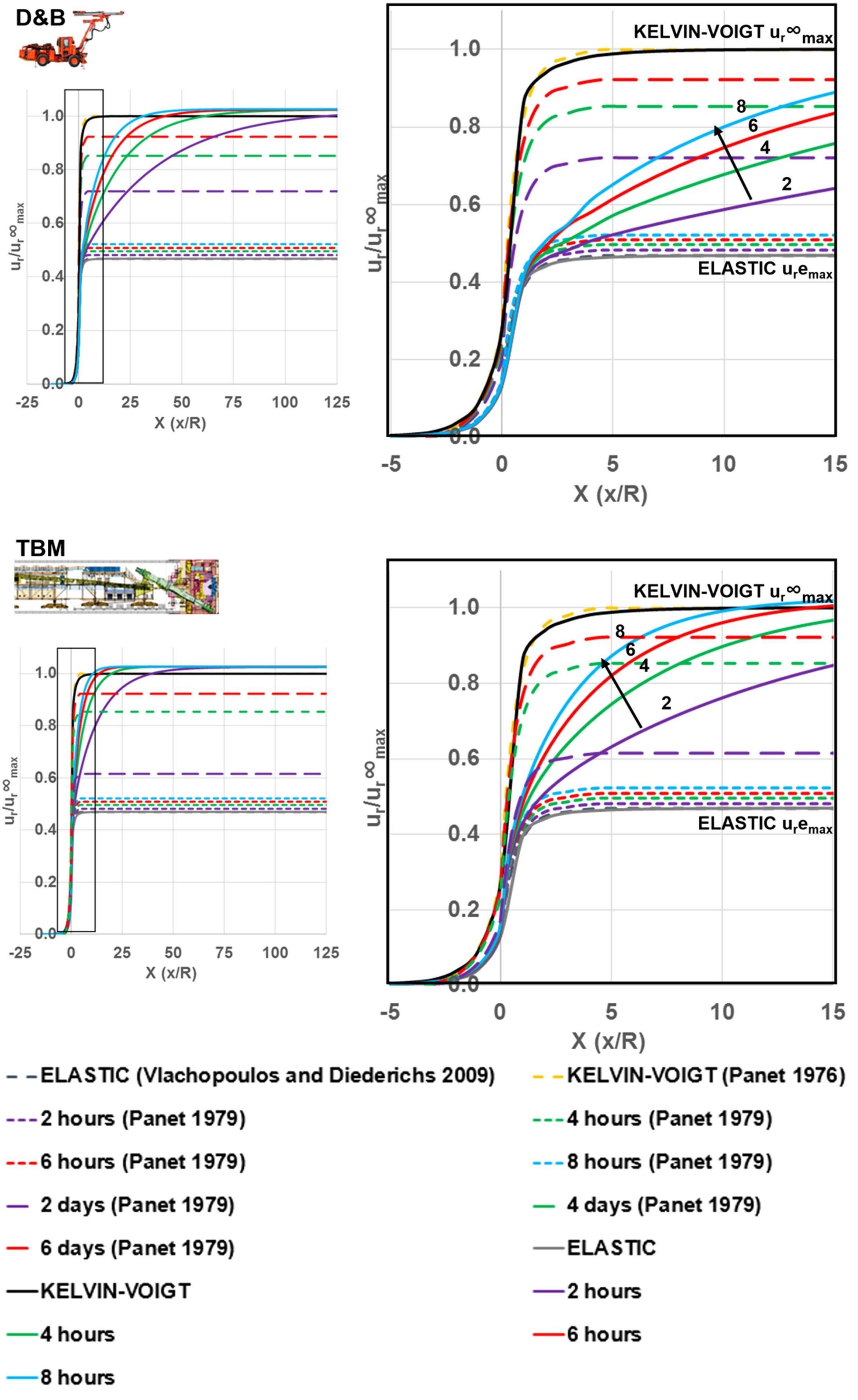

D&B
TBM
KELVIN-VOIGT $u_r\infty_{max}$
ELASTIC u_re_{max}
$u_r/u_r\infty_{max}$
X (x/R)
8
6
4
2
ELASTIC (Vlachopoulos and Diederichs 2009)
KELVIN-VOIGT (Panet 1976)
2 hours (Panet 1979)
4 hours (Panet 1979)
6 hours (Panet 1979)
8 hours (Panet 1979)
2 days (Panet 1979)
4 days (Panet 1979)
6 days (Panet 1979)
ELASTIC
KELVIN-VOIGT
2 hours
4 hours
6 hours
8 hours

TABLES

Table 1. Analytical solutions for LDP calculation depending on the medium.

Table 2. Visco-elastic rheological models, their associated mechanical analogues, stress-strain and time-relationships.

Table 3. Visco-elastic models and analytical solutions for a circular unsupported tunnel. The analytical solutions for Kelvin-Voigt and Maxwell model are adopted from Panet (1979) and for Burgers from Fahimifar et al. (2010).

Table 4. Parameters used for CVISC model.

Table 5. Nomenclature and model runs in this study.

Table 1. Analytical solutions for LDP calculation depending on the medium.

Reference	Analytical Solution	Medium Behaviour
Panet and Guenot (1982)	$\frac{u_r}{u_{max}} = 0.28 + 0.72[1 - (\frac{0.84}{0.84 + {}^{x}/_{R}})^2$	Elasto-Plastic
Panet (1993, 1995)	$\frac{u_r}{u_{max}} = 0.25 + 0.75[1 - \left(\frac{0.75}{0.25 + {}^{x}/_{R}}\right)^2]$	Elastic
Corbetta et al. (1991)	$\frac{u_r}{u_{max}} = 0.29 + 0.71[1 - \left(-1.5({}^{x}/_{R})^{0.7}\right)]$	Elastic
Chern et al. (1998)	$\frac{u_r}{u_{max}} = [1 + exp\left(\frac{-x/_R}{1.1}\right)^{-1.7}]$	Elasto-plastic
Unlu and Gercek (2003)	$\frac{u_r}{u_{max}} = \frac{u_o}{u_{max}} + A_a(1 - e^{B_a({}^{x}/_{R})}), \quad {}^{x}/_{R} \leq 0$ $\frac{u_r}{u_{max}} = \frac{u_o}{u_{max}} + A_b[1 - ((B_b + ({}^{x}/_{R}))^2], \quad {}^{x}/_{R} \geq 0$ $\frac{u_o}{u_{max}} = 0.22v + 0.19, \quad {}^{x}/_{R} = 0$ $A_a = -0.22v + 0.19 \quad B_a = 0.73v + 0.81$ $A_b = -0.22v + 0.81 \quad B_b = 0.39v + 0.65$	Elastic
Vlachopoulos and Diederichs (2009)	$\frac{u_r}{u_{max}} = \frac{u_o}{u_{max}} e^{{}^{x}/_{R}}, \quad {}^{x}/_{R} \leq 0$ $\frac{u_r}{u_{max}} = 1 - (1 - \frac{u_o}{u_{max}})e^{(-3x/_R)/({}^{2r_p}/_{R})}, \quad {}^{x}/_{R} \geq 0$ $\frac{u_o}{u_{max}} = \frac{1}{3}e^{-0.15\,({}^{r_p}/_{R})}, \quad {}^{x}/_{R} = 0$ r_p $- plastic\ radius$	Elasto-plastic

Table 2. Visco-elastic rheological models, their associated mechanical analogues, stress-strain and time-relationships.

Model	Mechanical Analogue	Stress-Strain – Time Relationships	
Kelvin	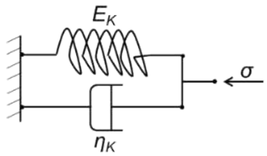	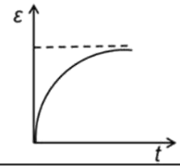	$\varepsilon(t) = \frac{\sigma}{E_K}\left[1-\exp\left(-\frac{E_K t}{3\eta_K}\right)\right]$
Maxwell	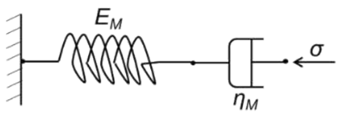	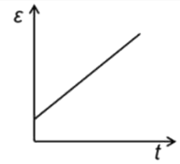	$\varepsilon(t) = \frac{\sigma}{E_M} + \frac{\sigma t}{3\eta_M}$
Generalized Maxwell	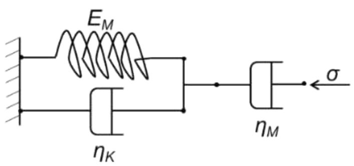	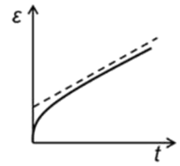	$\varepsilon(t) = \frac{\sigma}{E_K}\left[1-\exp\left(-\frac{E_K t}{3\eta_K}\right)\right] + \frac{\sigma t}{3\eta_M}$
Generalized Kelvin (Kelvin-Voigt)	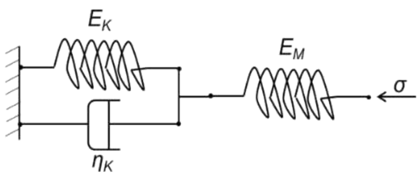	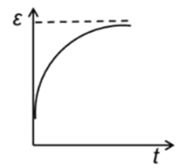	$\varepsilon(t) = \frac{\sigma}{E_M} + \left[1-\exp\left(-\frac{E_K t}{3\eta_K}\right)\right]$
Burgers	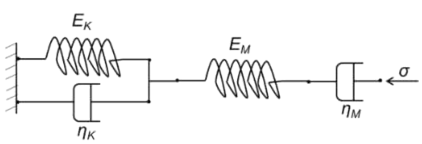	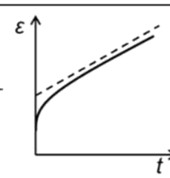	$\varepsilon(t) = \frac{\sigma}{E_M} + \left[1-exp\left(-\frac{E_K t}{3\eta_K}\right)\right] + \frac{\sigma t}{3\eta_M}$
CVISC	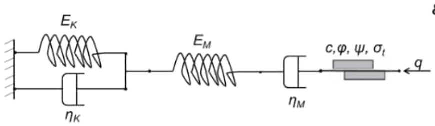	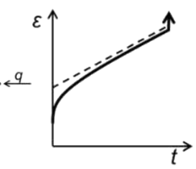	$\varepsilon(t) = \frac{p}{3K} + \frac{q}{3\,G_M} + \frac{q}{3\eta_M}\mathrm{t} + \frac{q}{3G_K} + \left[1-exp\left(-\frac{G_K}{\eta_K}\mathrm{t}\right)\right]$

(It should be noted that for incompressible materials E=3G).

Table 3. Visco-elastic models and analytical solutions for a circular unsupported tunnel (the analytical solutions for Kelvin-Voigt and Maxwell model are adopted from Panet (1979) and for Burgers from Fahimifar et al. (2010)).

<table>
<tr><th>Model</th><th>Spring-Dashpot Analogues and Radial displacement – Time Analytical Solutions</th></tr>
<tr><td>Kelvin-Voigt
(Generalized Kelvin)
(primary)</td><td>
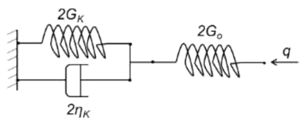

$\frac{1}{G_\infty}=\frac{1}{G_o}+\frac{1}{G_K}$

$T_K=\frac{\eta_K}{G_K}$

$u_r=\frac{\sigma_o r}{2G_o}+\frac{\sigma_o r}{2G_K}[1-\exp\left(-\frac{t}{T_K}\right)]$

$\sigma_r=0\ for\ t>0$

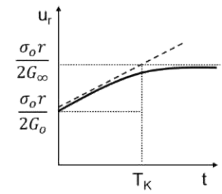

</td></tr>
<tr><td>Maxwell
(secondary)</td><td>
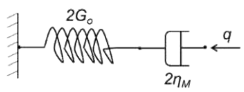

$T_M=\frac{\eta_M}{G_o}$

$u_r=\frac{\sigma_o r}{2G_o}[1+\left(\frac{t}{T_M}\right)]$

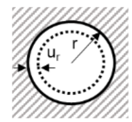

$\sigma_r=0\ for\ t>0$

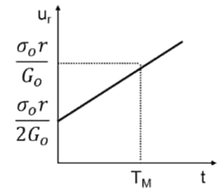

</td></tr>
<tr><td>Burgers
*(primary &
secondary)*</td><td>
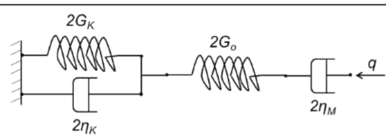

$\frac{1}{G_\infty}=\frac{1}{G_o}+\frac{1}{G_K}$

$T_K=\frac{\eta_K}{G_K}$

$u_r=\frac{\sigma_o r}{2}\{\frac{1}{G_o}+\frac{t}{\eta_M}+\frac{1}{G_K}[1-\exp\left(-\frac{t}{T_K}\right)]]\}$

$\sigma_r=0\ for\ t>0$

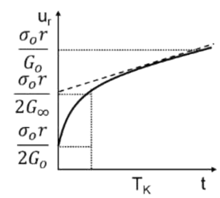

</td></tr>
</table>

Table 4. Parameters used for CVISC model.

Parameter	SET #1	SET #2	SET #3
Rockmass conditions			
γ (KN/m^3)	20	20	20
φ (^{o})	23	23	23
c (MPa)	1.00E+20	1.00E+20	1.00E+20
t (MPa)	1.00E+20	1.00E+20	1.00E+20
K (MPa)	1.23E+03	4.32E+04	4.70E+03
Stress Conditions			
k_0	1	1	1
p_0 (or σ_0) (MPa)	7	7	7
Visco-elastic Parameters*			
G_K (MPa)	4.98E+02	6.73E+04	3.29E+03
η_K(MPa*s)	1.34E+08	1.72E+09	1.49E+07
G_0 or G_M (MPa)	5.66E+02	1.99E+04	2.17E+03
η_M (MPa*s)	8.82E+08	1.20E+10	3.60E+09
$T_K = \eta_K/G_K$ (s)	2.69E+05	2.56E+04	4.52E+03
Reference*	Barla et al. 2010	Zhang et al. 2012	Feng et al. 2006

Table 5. Nomenclature and model runs in this study.

Model	Time per excavation cycle	CASE 1 - D&B (3m/exc.)			CASE 2 - TBM (3m/exc.)		
		SET#1	**SET#2**	**SET#3**	**SET#1**	**SET#2**	**SET#3**
KELVIN-VOIGT (KV)	2 hours	X	X	X	X	X	X
	4 hours	X	X	X	X	X	X
	6 hours	X	X	X	X	X	X
	8 hours	X	X	X	X	X	X
BURGERS (B)	2 hours	X	X	X	X	X	X
	4 hours	X	X	X	X	X	X
	6 hours	X	X	X	X	X	X
	8 hours	X	X	X	X	X	X
*KELVIN-VOIGT**	infinite excavation delay	X	X	X	X	X	X
*ELASTIC**	instantaneous excavation	X	X	X	X	X	X

**no time between excavation stages was considered in these models although in the KV model, both springs in series were considered active (zero viscosity in the Kelvin dashpot)*

LIST OF SYMBOLS - GLOSSARY

CCM	Convergence Confinement Method
CVISC	Burgers visco-plastic Model
LDP	Longitudinal Displacement Profile
GRC	Ground Reaction Curve
SCC	Support Characteristic Curve
E	Young's modulus
el	elastic
G or G_o	shear modulus
G_K	Kelvin shear modulus
G_M	Maxwell shear modulus
$1/G_\infty$	harmonic average
K	bulk modulus
p_0	in situ stress
p_i	internal pressure
q	deviatoric stress
q_{cr}	critical deviatoric stress
r	radius
r_p	plastic radius
R	tunnel radius
t	time
u_r	radial displacement
$u_r e_{max}$	maximum elastic displacement
$u_r{}^{\infty}{}_{max}$	maximum visco-elastic displacement
v	Poisson's ratio
v_e	visco-elastic
v_p	visco-plastic
x	distance from the tunnel face
y	yielding
η	viscosity
η_K	Kelvin viscosity
η_M	Maxwell viscosity
ε	strain
$\dot{\varepsilon}$	strain-rate
ε^p	axial strain due to primary stage of creep

ε^{s}	axial strain due to secondary stage of creep
ε^{tet}	axial strain due to tertiary stage of creep
σ	stress
σ_0	in situ stress
σ_r	radial stress
σ_{xx}	minor stresses
σ_{zz}	major stresses
T	denotes the retardation – relaxation time of each model